Icarus 206 (2010) 253–268

Contents lists available at ScienceDirect

Icarus

journal homepage: www.elsevier.com/locate/icarus

Hydrated mineral stratigraphy of Ius Chasma, Valles Marineris

Leah H. Roach [a,*], John F. Mustard [a], Gregg Swayze [b], Ralph E. Milliken [c], Janice L. Bishop [d], Scott L. Murchie [e], Kim Lichtenberg [f]

[a] Dept. Geological Sciences, Brown University, 324 Brook St., Providence, RI 02912, USA
[b] US Geological Survey, Branch of Geophysics, Box 25046, MS 964, Denver Federal Center, Denver, CO 80225, USA
[c] Jet Propulsion Laboratory, MS 183-30, 4800 Oak Grove Dr., Pasadena, CA 91109, USA
[d] The SETI Institute and NASA-Ames Research Center, Carl Sagan Center, 515 N. Whisman Rd., Mountain View, CA 94043, USA
[e] Applied Physics Laboratory, 11100 Johns Hopkins Rd., Laurel, MD 20723, USA
[f] Dept. Earth and Planetary Sciences, Washington University in St. Louis, 1 Brookings Dr., Box 1169, St. Louis, MO 63130, USA

ARTICLE INFO

Article history:
Received 8 May 2009
Revised 15 August 2009
Accepted 7 September 2009
Available online 19 September 2009

Keywords:
Mars, Surface
Spectroscopy

ABSTRACT

New high-resolution spectral and morphologic imaging of deposits on walls and floor of Ius Chasma extend previous geomorphic mapping, and permit a new interpretation of aqueous processes that occurred during the development of Valles Marineris. We identify hydrated mineralogy based on visible-near infrared (VNIR) absorptions. We map the extents of these units with CRISM spectral data as well as morphologies in CTX and HiRISE imagery. Three cross-sections across Ius Chasma illustrate the interpreted mineral stratigraphy. Multiple episodes formed and transported hydrated minerals within Ius Chasma. Polyhydrated sulfate and kieserite are found within a closed basin at the lowest elevations in the chasma. They may have been precipitates in a closed basin or diagenetically altered after deposition. Fluvial or aeolian processes then deposited layered Fe/Mg smectite and hydrated silicate on the chasma floor, postdating the sulfates. The smectite apparently was weathered out of Noachian-age wallrock and transported to the depositional sites. The overlying hydrated silicate is interpreted to be an acid-leached phyllosilicate transformed from the underlying smectite unit, or a smectite/jarosite mixture. The finely layered smectite and massive hydrated silicate units have an erosional unconformity between them, that marks a change in surface water chemistry. Landslides transported large blocks of wallrock, some altered to contain Fe/Mg smectite, to the chasma floor. After the last episode of normal faulting and subsequent landslides, opal was transported short distances into the chasma from a few m-thick light-toned layer near the top of the wallrock, by sapping channels in Louros Valles. Alternatively, the material was transported into the chasma and then altered to opal. The superposition of different types of hydrated minerals and the different fluvial morphologies of the units containing them indicate sequential, distinct aqueous environments, characterized by alkaline, then circum-neutral, and finally very acidic surface or groundwater chemistry.

1. Introduction

Valles Marineris is a dominant feature in the western hemisphere of Mars – 4000 km long and up to 7 km deep – that has inspired many hypotheses for its formation (e.g. McCauley et al., 1972; Tanaka and Golombek, 1989; Lucchitta et al., 1992). Orbiting spectrometers have discovered large exposures of a variety of minerals within Valles Marineris, from olivine and other basaltic components (Mustard et al., 1997; Christensen et al., 2005, 2003) to alteration minerals including sulfate (Gendrin et al., 2005), hematite (Fe_2O_3) (Christensen et al., 2001), and other ferric phases (Bibring et al., 2007). Recent CRISM discoveries include opal (Milliken et al., 2008; Weitz et al., 2008) and phyllosilicates (Murchie et al., 2009a) within and surrounding Valles Marineris. Water played an important role in both the formation of Valles Marineris and its associated outflow channels and in creating these alteration minerals (Gendrin et al., 2005; Murchie et al., 2009a). However, the different chemical alteration products within Valles Marineris are newer discoveries (e.g. Gendrin et al., 2005; Milliken et al., 2008; Murchie et al., 2009a,b; Bishop et al., 2009; Roach et al., 2009) and their relative timing is not well understood.

Exposures of different geologic units within Ius Chasma are ideal for probing the possible occurrence of different chemical environments during the formation of Valles Marineris. Studying the mineralogy of materials in Ius Chasma can help shed more light onto fluvial processes and constrain the timing of phyllosilicate alteration. Examining the close spatial relationship between

* Corresponding author.
E-mail address: leah_roach@brown.edu (L.H. Roach).

0019-1035/$ - see front matter © 2009 Elsevier Inc. All rights reserved.
doi:10.1016/j.icarus.2009.09.003

sulfate and smectites can also help resolve questions about their relative timing and respective formation processes. With geomorphic and mineralogic evidence, we build on previous structural and surficial geologic mapping to construct a more detailed history of aqueous processes in this area of Mars.

2. Background

2.1. Geologic history

The origin of the Valles Marineris canyon system has been an area of intense research since its discovery (e.g., McCauley et al., 1972; Sharp, 1973; Carr, 1974; Lucchitta et al., 1992, 1994). Several mechanisms have been proposed to explain its formation, including karst-style collapse, erosional, and tectonic processes (e.g., McCauley et al., 1972; Blasius et al., 1977; Croft, 1989; Tanaka and Golombek, 1989; Lucchitta et al., 1990; Schultz, 1998). The currently favored model invokes extension due to tectonic stress related to the Tharsis Rise, although the details are under debate (Mege and Masson, 1996 and references therein).

The structural control of landform development is striking in Ius Chasma (Fig. 1), where several features are evidence of the repeated tensional and erosional events. First, the wallrock often exhibits triangular faceted spurs where linear fault scarps cut the spur-and-gully topography (Hamblin, 1976; Blasius et al., 1977). Secondly, the central ridge, Geryon Montes, is interpreted as a horst between the two grabens of north and south Ius Chasma (Peulvast and Masson, 1993a). Finally, the sapping channels that comprise Louros Valles along the southern wall have two preferred orientations (Kochel and Piper, 1986). These orientations demonstrate the structural control that influences both the sapping channels and fracturing along the chasma (Kochel and Piper, 1986). The creation of structural weaknesses exploited by sapping channels and other fracturing is thought to predate the formation of Valles Marineris (Tanaka, 1986).

A detailed geologic history of Ius Chasma has been established from imaging and topographic data (e.g., Tanaka, 1986; Peulvast and Masson, 1993a,b; Peulvast et al., 2001). The region consists of a megabrecciated basement (Tanaka and Golombek, 1989) overlain during the Late Noachian period by lava flows that accumulated to several kilometers in thickness (Lucchitta et al., 1992; Tanaka et al., 1992; McEwen et al., 1999; Williams et al., 2003). The elevation of the contact between Hesperian and Noachian materials is uncertain, but the Hesperian volcanics are at least several kilometers thick in the Ius Chasma region. These Late Noachian – Early Hesperian lava plains were part of the voluminous Tharsis volcanism (Tanaka et al., 1991) and are interpreted to be cut by multiple dikes or lithified faults (Lucchitta et al., 1992). The ~400 m thick, uppermost layer of the lava flows is more resistant to erosion than underlying layers and may be evidence of aqueous alteration or cementation during the Late Hesperian period (Treiman et al., 1995; McEwen et al., 1999).

Valles Marineris formed over a long period from Early to Late Hesperian following the accumulation of the thick lavas (Tanaka, 1986), and multiple processes likely contributed to its geometry. It is possible that wider, more irregular chasmata, such as Capri and Melas Chasma, formed in subsiding ancestral basins (Lucchitta et al., 1994; Schultz, 1998). Long rectangular troughs, including Ius Chasma, developed as grabens that eventually connected to the wider chasmata (Lucchitta and Bertolini, 1989; Peulvast and Masson, 1993a,b). Ius Chasma may have been isolated from Melas Chasma to the east during its earliest stages (Peulvast and Masson, 1993a). Mass wasting of wallrock widened the chasma. Large outflow channels debouched at the eastern end of Valles Marineris during the middle Hesperian period, but did not leave fluvial features in Ius Chasma either because the bulk of the water originated eastward of Ius, or because later deposition, faulting, and landslides obscured those features.

Geryon Montes divided Ius Chasma into northern and southern sub-basins early in the chasma's history, yet retains possible evidence for how the horst and graben topography initiated. Geryon Montes has several linear ridges ~10–20 km in length along its crest, variously interpreted as mafic dikes (Ernst et al., 2001), the result of slow mass wasting (Peulvast et al., 2001), or fault zones cemented by groundwater (Treiman, 2008). Dike formation is the most likely explanation. Mass wasting of a narrow horst would not obviously create multiple linear ridges, but would tend to form one crest, and in cases of asymmetry in horst geometry or rainfall, create arcuate crests (Ellis et al., 1999). Water-deposited mineral cements in fault zones also do not satisfactorily explain the linear ridges. These ridges are 5.5 km above the trough floor and 2.5 km below the surrounding plateau; an enormous amount of water would be necessary to have groundwater cementation of these faults. Additionally, the texture and albedo of these linear ridges do not differ from other wallrock ridges, and, though not dust covered, lack evidence of hydrated mineralogy in CRISM spectra. The ridges are similar in character to the rest of the layered volcanic rocks in Geryon Montes. The major volcano-building activity in Tharsis Rise created multiple radial dike swarms, and the linear ridges in Geryon Montes may be part of a Noachian-aged swarm (Ernst et al., 2001). The putative dikes also align with the sapping channel orientations and are nearly parallel with the trough's strike. Thus, the fractures controlling these features formed before Valles Marineris opened and could be part of the tectonic stress regime that predated Tharsis as well (Tanaka, 1986; Lucchitta et al.,

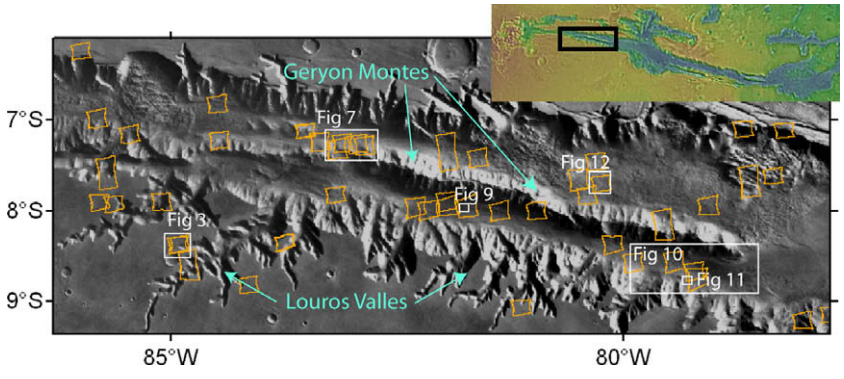

Fig. 1. MDIM of linear Ius Chasma showing sapping channels, spur-and-gully erosional topography on wallrocks, and structurally controlled fractures. CRISM outlines included in study in orange. White boxes indicate locations of geologic contacts shown in Figs. 3, 7 and 9–12. Inset: location of Ius Chasma within Valles Marineris (colored MOLA). (For interpretation of the references to colour in this figure legend, the reader is referred to the web version of this article.)

1992). Dike intrusion into the future Geryon Montes may have locally strengthened that rock by filling fractures or partially annealing the layered volcanic flows and underlying regolith. A similar linear ridge runs along the crest of the central horst in Coprates Chasma (Treiman, 2008). It is possible that dike intrusions help facilitate horst and graben formation under extensional stress (McKenzie and Nimmo, 1999).

After initial rifting, the walls of Ius Chasma were extensively modified by fluvial erosion and mass wasting–forming spur-and-gully morphology, sapping channels, and landslide scars. The "spur-and-gully" morphology in Ius Chasma was developed by streams cutting across fault scarps (Lucchitta et al., 1992). The spur-and-gully morphology is visible on the interior ridge of Geryon Montes and on wall material not later cut by sapping channels and landslides. It is not found re-developing on landslide scars, so either the landslides were too recent to allow spur-and-gully erosion, or the spur-and-gully morphology was developed in an early, possibly wetter, environment (Lucchitta et al., 1992). The level of dissection is dependent on rock strength and amount of fluvial erosion (Ellis et al., 1999). Normal faulting during spur-and-gully formation resulted in hanging triangular facets along the north wall of north Ius Chasma, eroded by continued incision of the catchments. Later normal faulting after spur-and-gully formation ceased preserved those triangular facets (Hamblin, 1976; Ellis et al., 1999). In addition to spur-and-gully morphology, fluvial erosion also formed sapping channels on both the northern and southern chasma walls. It is most noticeable in Louros Valles, which is interpreted as a collection of sapping channels each 30–130 km long. The sapping channels were active into the Early Amazonian (Craddock and Howard, 2002), and they uniformly cut spur-and-gully features (Peulvast et al., 2001). Finally, landslide deposits cover much of the trough floor. Crater counting of five landslides in eastern Ius Chasma produced dates ranging from 60 to >1000 Myr, suggesting episodic landslide activity from the initial rifting until the present (Quantin et al., 2004).

Normal faulting in Ius Chasma continued from the late Hesperian through late Amazonian periods, and the cross-cutting relations of these faults with mineral deposits and erosional features can determine the relative timing and duration of different processes (Peulvast et al., 2001). Landslides and sapping channels both transect and are transected by faults. Faulting in Ius can generally be divided into "earlier" and "later" faulting, occurring either during spur-and-gully formation or after it had ceased. The "later" faulting caused preferentially more slip along the base of northern walls than southern walls in both the northern and southern subbasins (Peulvast et al., 2001). This could be due to an asymmetric graben. Although "later" faulting only accounts for ~10% of the total canyon wall relief, it was an important period that likely widened the connection between Ius and Melas Chasmata (Peulvast et al., 2001). There is also evidence for aqueous processes on the plateau around Ius Chasma. Opal deposits on the plateau south of Ius and Melas Chasmata formed during the late Hesperian and early Amazonian periods (Milliken et al., 2008; Weitz et al., 2008). The drainage networks on the plains north west of Ius and within Melas Chasma may be caused by Hesperian-aged precipitation and surface runoff (Weitz et al., 2003; Mangold et al., 2004).

2.2. Mars Reconnaissance Orbiter (MRO) datasets

The Compact Reconnaissance Imaging Spectrometer for Mars (CRISM) instrument is a visible-infrared hyperspectral imaging spectrometer capable of acquiring observations in both ~20 m/pixel targeted and 100–200 m/pixel mapping modes (Murchie et al., 2007). The spectra include compositional information due to charge transfer and electronic transition absorptions due to transition metal elements (especially Fe) in materials, and vibrational overtones and combination tones of anions including OH^-, SO_4^{2-}, and CO_3^{2-} in coordination with cations of Si, Mg, Fe, etc. (Burns, 1993; Clark et al., 1990).

Two cameras are coaligned with CRISM on the MRO spacecraft: the High Resolution Imaging Science Experiment (HiRISE) and the Context Camera (CTX). HiRISE acquires very high resolution (up to 25 cm/pixel) imagery, sufficient to resolve the fine layering and polygonal fracturing in many of the hydrated materials (McEwen et al., 2007). CTX images are ~6 m/pixel and ~30 km across, well-suited for compiling high spatial resolution mosaics covering large areas (Malin et al., 2007). Many of the CRISM observations are accompanied by simultaneous HiRISE and CTX images for coordinated analysis of surface composition and morphology.

2.3. MOLA topography

The Mars Orbiter Laser Altimeter (MOLA) on the MGS spacecraft collected shot data with a 160 m surface spot size and 300 m spacing between shots (Zuber et al., 1992). These data were aggregated into a global 128 pixel/degree grid with a vertical accuracy of <30 m (Zuber et al., 1992; Smith et al., 2003). This gridding results in 460 m/pixel spacing near the equator. In regions with rapid elevation changes and with dense shot distribution, such as Ius Chasma, shot data is preferable for its higher accuracy than gridded data, but is limited to the acquired orbital tracks. MOLA shot data is ideal for creating detailed stratigraphic cross-sections of the surface deposits in Ius Chasma.

3. Methods

3.1. CRISM data reduction

CRISM data are reduced to atmospherically corrected apparent surface reflectance via a standard calibration pipeline (Murchie et al., 2007, 2009c). An optional further step is to "clean" the data in the spectral and spatial dimensions to remove instrumental noise and column-to-column variation (Parente, 2008). Both "cleaned" and "uncleaned" spectra were analyzed in this study.

3.2. Spectral interpretation of minerals

Spectral summary parameters are calculated from diagnostic absorptions to aid preliminary identification of minerals and atmospheric components as described in Pelkey et al. (2007). Parameters for hydrated sulfate and phyllosilicate minerals were particularly useful (see Table 1 for formulations). Summary parameters used in this study include the 1.9 μm band depth, due to combinations of H_2O bending and stretching vibrations (BD1900); the 2.1 μm band depth, due to H_2O vibrational combinations (BD2100); the 2.21–2.26 μm band depth, due to Si-OH vibrations (BD2210); the 2.3 μm band depth, due to metal-OH vibrations (D2300); and the convexity around 2.3 μm in very hydrated phases due to strong H_2O absorptions at 1.9 and 3 μm (SINDEX). These summary parameters are useful for sifting through large amount of spectral data to identify areas that warrant more detailed analysis, and for mapping out regions with aqueous minerals, but they are not sufficient by themselves for mineral identification.

Further analysis including at least the 0.4–2.6 μm wavelength range in both corrected I/F and ratioed spectra is necessary to determine the presence of a specific mineralogy. Typically, corrected I/F spectra are averaged into at least 3 × 3 or 5 × 5 pixel aggregates to reduce instrumental noise. A spectrum of interest is also divided by a spectrum of a spectrally neutral (i.e. dusty) region to accentuate subtle mineral absorption bands and to remove residual instrumental artifacts. If ratioing is performed, the spectrally neutral denominator spectrum should come from the same column(s) as the

Table 1
Hyperspectral parameters for indicating hydrated mineralogy.

Spectral parameter	Formulation	Features identified
BD1900R	$1-[(R1908+R1914+R1921+R1928+R1934+R1941)/(R1862+R1869+R1875+R2112+R2120+R2126)]$	1.9 μm Absorption due to combinations of H_2O bending and stretching vibrations
BD2100	$1-[(0.5*(R2120+R2140))/(b*R1930+a*R2250)]$ $a=(R2120-R1930)/(R2250-R1930)$; $b=1-a$	2.1 μm H_2O vibrational combinations in monohydrated sulfates
BD2210	$1-[R2210/(b*R2140+a*R2250)]$ $a=(R2210-R2140)/(R2250-R2140)$; $b=1-a$	Si-OH vibrations around 2.21 μm
D2300	$1-[(R2290/CR2290)+(R2320/CR2320)+(R2330/CR2330)/(R2120/CR2120)+(R2170/CR2170)+(R2210/CR2210)]$	Metal-OH vibrations around 2.3 μm
SINDEX	$1-[(R2100+R2400)/(2*R2290)]$	Convexity around 2.3 μm due to H_2O absorptions at 1.9 and 3 μm

Where $R1908$ indicates the reflectance at 1.908 μm and $CR2290$ indicates the calculated continuum reflectance at 2.29 μm from a fit to a line from 1.80 to 2.53 μm.

spectrum of interest to account for column-dependent wavelength calibration (Murchie et al., 2007, 2009c). A spectrally neutral denominator is best, as mineral absorptions in the denominator show up as inverse features in ratioed spectra and can complicate mineral identification. Ratioed spectra then are compared to the laboratory data of pure minerals for potential matches.

Hydrated minerals, including hydrated silica, sulfates, phyllosilicates, and carbonates, all show a pronounced ~1.9 μm absorption due to H_2O (Hunt et al., 1971, 1973), so other absorptions are necessary to resolve which class of hydrated mineral is present (Fig. 2B). Monohydrated sulfates, such as kieserite ($MgSO_4{\cdot}H_2O$) and szomolnokite ($Fe^{2+}SO_4{\cdot}H_2O$), have absorptions near 2.1 μm (with the exact minimum varying by cation) and near 2.4 μm (Cloutis et al., 2006). The 2.1 μm absorption, which is due to a combination of H_2O stretch and rotation vibrations, is closer to 2.13 μm in natural kieserite and 2.09 μm in szomolnokite (Cloutis et al., 2006; Crowley et al., 2003). Szomolnokite also has a broad ferrous crystal field absorption at 0.94 μm (Crowley et al., 2003). Polyhydrated sulfates (e.g., hexahydrite $MgSO_4{\cdot}6H_2O$) have strong H_2O vibrations at 1.45 and 1.95 μm as well as a drop off in reflectance near 2.45 μm attributed to a strongly hydrogen bonded OH/H_2O combination band (Cloutis et al., 2006).

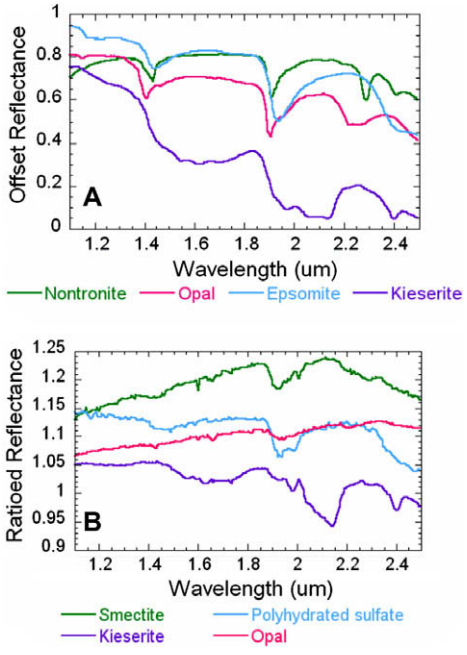

Fig. 2. (A) CRISM ratioed spectra of hydrated minerals identified within Ius Chasma. (B) RELAB library reflectance spectra of relevant hydrated minerals: hexahydrite ($MgSO_4{\cdot}6H_2O$), nontronite and opal.

Multiple hydrated minerals have diagnostic absorptions in the 2.2–2.3 μm region. Hydrated silica is identified by minima at 1.38–1.46 and 2.20–2.26 μm, which are attributed to a combination of the OH stretching fundamental with an Si-OH (silanol) bending mode (Anderson and Wickersheim, 1964). The 2.20 μm feature is due to silanol vibrations, whereas the 2.26 μm is due to vibration of silanol groups hydrogen bonded to free waters of hydration (Anderson and Wickersheim, 1964). Hydroxylated silica without free water will only have a 2.20 μm absorption, whereas hydrated samples show a broad absorption between 2.20 and 2.26 μm that is composed of several overlapping bands. The 2.20 μm absorption is always stronger than the 2.26 μm absorption (Anderson and Wickersheim, 1964). In addition to classifying by the presence/absence of free water, hydrated silica can be classified into opal-A (disordered), opal-C, and opal-CT, where the latter two contain ordered domains of crystalline cristobalite or cristobalite and tridymite (Smith, 1998). Spectral signatures are similar between opal subtypes with excess waters of hydration (Goryniuk et al., 2004; Milliken et al., 2008), and for clarity with other minerals discussed in this paper, we refer in this paper to all hydrated silica phases as "opal." Jarosite ($KFe_3^{3+}(OH)_6(SO_4)_2$) and gypsum ($CaSO_4{\cdot}2H_2O$) also have absorptions in the 2.2 μm region, but are distinguished from opal by other VNIR absorptions. Jarosite exhibits absorptions at 1.47 and 1.85 μm due to hydroxyl combination vibrations, and a doublet at 2.21 and 2.26 μm due to Fe-OH vibrations (Crowley et al., 2003). Gypsum has a distinctive triplet absorption between 1.44 and 1.54 μm, absorptions at 1.75 and 1.9 μm, and a doublet at 2.25 and 2.265 μm, all due to combinations and overtones of H_2O vibrations and librations (Hunt et al., 1971; Cloutis et al., 2006). The smectite clays have a narrow metal-OH absorption in the 2.3 μm region, whose minimum moves from 2.31 μm for Mg-rich saponite to 2.28 μm for Fe-rich nontronite to 2.20 μm for Al-rich montmorillonite/beidellite (Bishop et al., 1994, 2008; Gates, 2005).

In this paper we focus on the presence, not the abundance, phases with visible-infrared spectral signatures. NIR spectrally neutral minerals, like quartz (SiO_2) or plagioclases ($MAlSi_3O_8$), may also be present. Variations in grain size, texture, and admixture with darkening agents or other minerals can all complicate retrieving abundances. Abundance calculations are not yet available for CRISM mineral identifications, although preliminary modeling efforts with OMEGA data are promising (e.g. Poulet et al., 2009a,b).

3.3. MOLA slope estimations

The slope of the plane of contacts between hydrated mineral deposits was defined as the slope of MOLA shot data running perpendicular to the contacts. Slopes were calculated over a single orbit of MOLA shot data, then several of these results were averaged

together for more robust estimates. MOLA shot data is relatively dense in the study region and dozens of orbits of MOLA shot data were available. Those orbits with MOLA data points closest to the mapped contact were used. While the contacts are much smaller than the MOLA footprint and the MOLA instrument's spatial accuracy, the estimates of slope, θ, for small angles are reasonably robust. For small angles, $\tan(\theta) \sim \theta$, so $\theta \sim y/x$ (vertical over horizontal distance). Thus, a 10% error in height results in a 10% error in slope, and a 10% error in vertical distance results in a 9.1% error in slope. For the estimated slopes of 10° on the Ius Chasma floor, the error is 1°.

4. Results

4.1. Spectral results

Fe/Mg smectite clay minerals, opal, and sulfates, including kieserite and a polyhydrated sulfate with an unspecified cation are all identified in light-toned deposits within Ius Chasma (Fig. 2A, Table 2). The Fe/Mg smectite clay was identified by its hydration bands at 1.40–1.44 and 1.91–1.92 μm, and a narrow minimum between 2.28 and 2.31 μm indicative of bend and stretch combinations of the the FeFeOH and the Mg_3-OH vibrations respectively (Madejova et al., 2008). The Fe/Mg smectite clay signature in Ius Chasma has a minimum near 2.29 μm, which is more consistent with Fe-bearing nontronite than Mg-bearing saponite and indicates an Fe-rich smectite clay. Opal is identified by absorptions at 1.42, 1.92, and a broad asymmetric-right absorption centered at 2.20 μm (Fig. 3A). The opal lacks the broader 2.26 μm minimum seen in the opal library spectrum since it has less waters of hydration. Kieserite is distinguished by its broad 1.65 μm, strong asymmetric-left 2.13 μm, and 2.39 μm absorptions. Polyhydrated sulfate has distinct absorptions at 1.43–1.45 and 1.91–1.95 μm and a drop off in reflectance around 2.4 μm. Pyroxene-bearing sand dunes (identified from broad 1- and 2-μm absorptions) and dust partially overlie some of these light-toned deposits. The wallrock, which shows mafic signatures elsewhere in Valles Marineris, is generally dusty and lacks strong spectral features in Ius Chasma. No ferric oxide separate from those in the globally-homogeneous dust was identified in the Ius deposits using CRISM data from 0.4 to 1.0 μm.

A hydrated mineral phase not previously seen on Mars was also detected and mapped in this region using CRISM data (Fig. 4). The material exhibits molecular H_2O absorptions at 1.40–1.42 and 1.91–1.92 μm and a sharp doublet attributed to metal-OH vibrations with minima at 2.205–2.218 and 2.265–2.278 μm. The relative depths of the 2.21 and 2.27 μm absorptions vary, but both absorptions are always present and have similar widths. Spectra of this phase can also exhibit a step or minor absorption near 2.4 μm. This phase is found in light-toned deposits elsewhere in Valles Marineris (the floors of southern Melas Chasma, Coprates Chasma, and Noctis Labyrinthus, and the central horst in Coprates Chasma), often in association with other hydrated minerals such as Fe/Mg smectite clays.

This newly recognized hydrated mineral phase does not correspond to any single mineral whose spectra are available in the RELAB or USGS spectral libraries (Clark et al., 2007). Mineral types investigated include sulfates, phyllosilicates, carbonates, chlorides, zeolites, phosphates, and opal. The closest spectral matches are jarosite, gypsum, opal, or a combination of hydrated phases such as smectite clay plus jarosite (Fig. 4). There are four hypotheses for the mineralogy that causes these absorptions: (1) sulfates structurally similar to gypsum or jarosite, perhaps in a mixture, (2) opal mixed with Fe/Mg smectite, possibly as a result of acid leaching of smectite, (3) a combination of Al- and Fe/Mg-bearing smectites, and (4) poorly crystalline mixed Al-ferric clay formed from acid alteration of Fe/Al smectite clay. These hypotheses are discussed in depth in Section 5.1. In subsequent mapping, this phase is called hydrated silicate, although it may in fact represent or include another mineral class.

4.2. Stratigraphic results

The spectral identifications in individual CRISM observations have been classified into geologic units (Table 2) and extended into a regional unit map (Fig. 5). First, CRISM targeted and multispectral mapping data were used to identify the locations of different hydrated phases. HiRISE and CTX images of those regions were examined to see if units have a characteristic morphology and to determine superposition relationships with adjacent geologic units. Many of the hydrated units are high-albedo, massive deposits that are indistinguishable from each other in HiRISE or CTX imagery, although they are distinct from surrounding dusty floor material and mafic wallrock outcrops. For example, the polyhydrated sulfate and massive hydrated silicate-bearing units are morphologically very similar, and in locations lacking spectral coverage, they cannot be confidently distinguished by imagery alone. Thus, detailed stratigraphic analysis is limited to locations covered

Table 2
Distinguishing spectral absorptions and descriptions of geologic units identified in Ius Chasma, Valles Marineris.

Geologic unit	Code	Spectral absorptions	Description
Kieserite	Kies	Broad 1.65, 2.13, 2.39 μm	Light-toned, massive unit, >200 m thick
Polyhydrated sulfate	PHS	1.43–1.45, 1.91–1.95, Drop off ~2.4 μm	Light-toned, massive unit, polygonal meterscale fracturing, >500 m thick
Massive hydrated silicate	Sil	1.40–1.42, 1.91–1.92, Sharp doublet at 2.205–2.218 and 2.265–2.278, sometimes ~2.4 μm	Light-toned, thin, massive unit, weathers into rough, orange peel-like texture
Layered sedimentary Fe/Mg smectite	Smec	1.40–1.44, 1.91–1.92, 2.29 μm	Finely layered to HiRISE resolution, meterscale polygonal fracturing
Sedimentary opal	OpalS	1.42, 1.92, Broad absorption between 2.17 and 2.30 μm centered at 2.20 μm	Intermediate to light-toned, tens meter thick, meterscale polygonal fracturing on plains around Valles Marineris
Transported opal	OpalT	1.42, 1.92, Broad absorption between 2.17 and 2.30 μm centered at 2.20 μm	Intermediate to light-toned, lobate morphology at base of sapping channels
Landslide with hydrated silicate(s)	Lh	1.40–1.42, 1.91–1.92, Sharp doublet at 2.205–2.218 and 2.265–2.278, sometimes ~2.4 μm	Breccia blocks up to 100 m across. Hydrated silicate in both breccia and cement
Landslides	L	Spectrally neutral	Morphologically similar to above, but without hydrated silicate signature
Wallrock	Wall	Spectrally neutral	Layered, intermediate-toned material exposed on sides of chasma and central ridge, with fluted spur-and-gully erosion
Undivided floor material	Undiv	Pyroxene (broad ~1 and ~2 μm) or dust	Pyroxene-bearing dark dunes, or dusty capping material

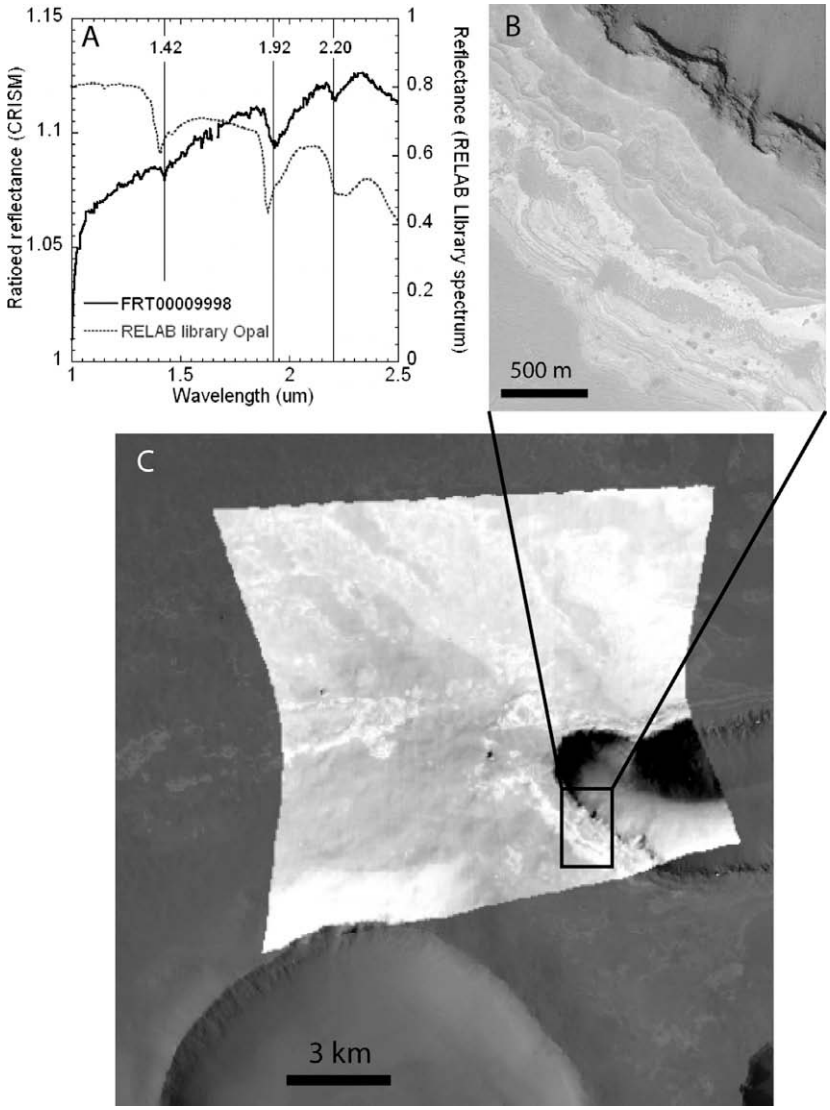

Fig. 3. (A) CRISM ratioed spectrum from FRT00009998 and RELAB library spectrum of opal. Both show the 2.21 μm absorption due to Si-OH vibrations. Library spectrum has an additional absorption at 2.26 due to free waters of hydration which the CRISM spectrum lacks. (B) HiRISE PSP_005215_1715 subset showing fine layering in hydrated silica. (C) CRISM FRT00009998 of Louros Valles over CTX P06_003237_1734. Part of ~10 km diameter crater visible in SW part of image.

by CRISM targeted observations. In places where the geologic unit identification and stratigraphy is clear in CTX data, those morphologic indicators are used for geologic mapping outside the extent of CRISM observations. The resulting regional unit map (Fig. 5) shows the broad extent of hydrated mineralogy on the Ius Chasma floor. Three inferred stratigraphic cross-sections show the relationships between the different geologic units.

Cross-section A–A′ (Fig. 6) shows the relationship of the hydrated silica, Fe/Mg smectite, and hydrated silicate with the wallrock and plains material. In the southern sub-basin, the opal-bearing material appears at the base of the sapping channels and in the lowest layers of the light-toned plateau deposits above Louros Valles (Fig. 3) (Weitz et al., 2008; Milliken et al., 2008). The floor deposits are cut by normal faulting, interpreted to be continued faulting of a graben underlying the floor of the southern Ius Chasma sub-basin (Peulvast and Masson, 1993b). Trace amounts of opal are also seen at the base of another sapping channel, 240 km away, overlying a polyhydrated sulfate deposit. A dozen other observations of Louros Valles headwalls show a similar thin, light-toned layer in the top few meters of the wallrock, but small exposures and dust cover complicate retrieving clean spectra. While several show weak hydration bands, none of them have spectra clearly identifiable as hydrated silica. We interpret the entire region cut by the Louros Valles sapping channels to be capped by a thin deposit that contains opal in the lowest layers, of unknown amount (Milliken et al., 2008; Weitz et al., 2008).

In the northern basin, cross-section A–A′ shows Fe/Mg smectite alteration in layered Geryon Montes material near −2000 m elevation (shown in perspective in Fig. 7, ~10 km east of the cross-section). At the base of this outcrop is a finely layered sedimentary Fe/Mg smectite deposit that drapes the lowest elevations. A massive hydrated silicate unit unconformably overlays the sedimentary Fe/Mg smectite unit. The surface expression of Fe/Mg smectite alteration in Geryon Montes is likely obscured by mass wasting. The "?" in Fig. 6 beneath Geryon Montes expresses the uncertainty of the depth of smectite alteration in Noachian basement rocks. Unlike in the southern sub-basin, scars from "recent" normal faulting of the graben underlying the northern sub-basin are not visible; the hydrated deposits are not cut by late stage tectonic activity.

Cross-section B–B′ (Fig. 8A) details the relative stratigraphy of the opal, layered sedimentary Fe/Mg smectite clay, and massive

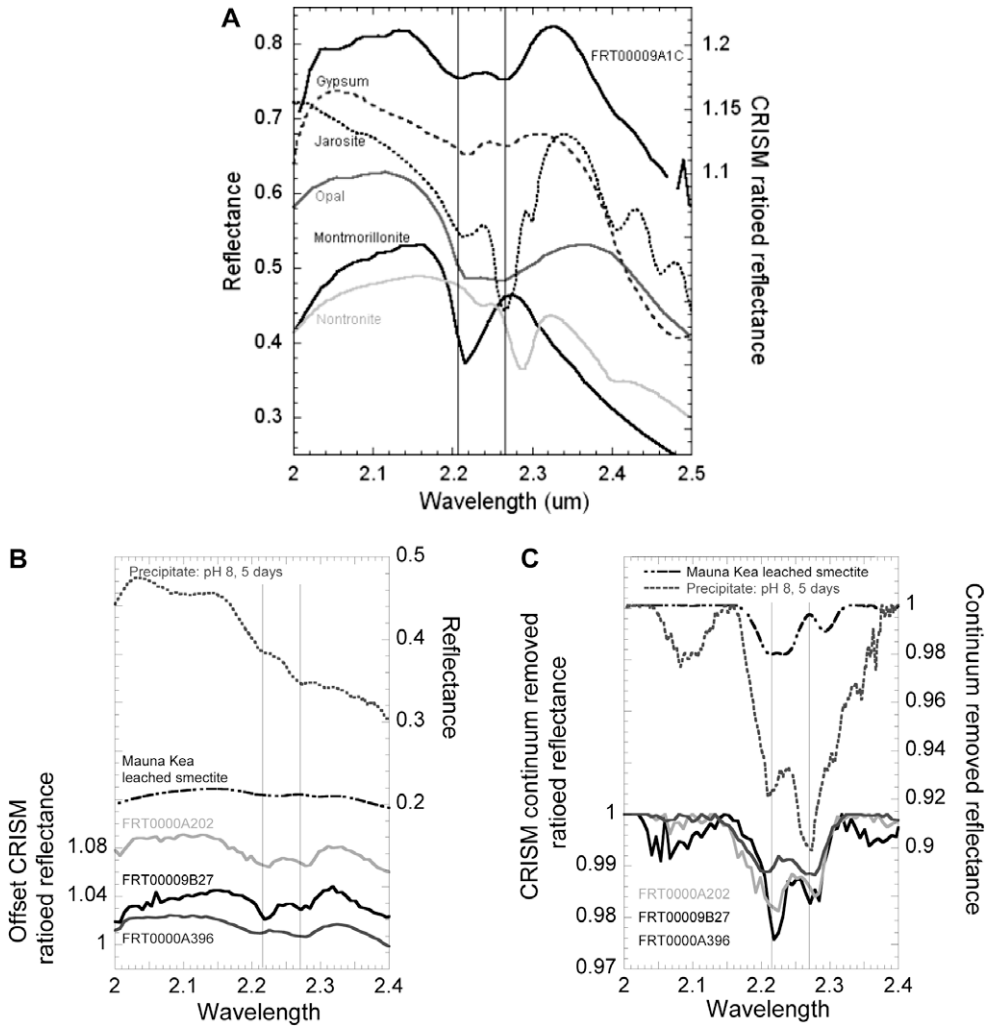

Fig. 4. (A) Cleaned spectrum from CRISM FRT00009A1C of 5387 pixels with RELAB library spectra of possible mineral components – gypsum, jarosite, opal, montmorillonite, and nontronite. Vertical lines at 2.207 and 2.266 μm. (B) Spectra of precipitated phase created by Tosca et al. (2008) and leached smectite clay from Mauna Kea compared to three representative CRISM spectra (FRT0000A202, FRT00009B27, and FRT0000A396) with a 2.21 and 2.27 μm doublet. Vertical lines at 2.215 and 2.27 μm. (C) Same spectra as in (B), with continuum removal.

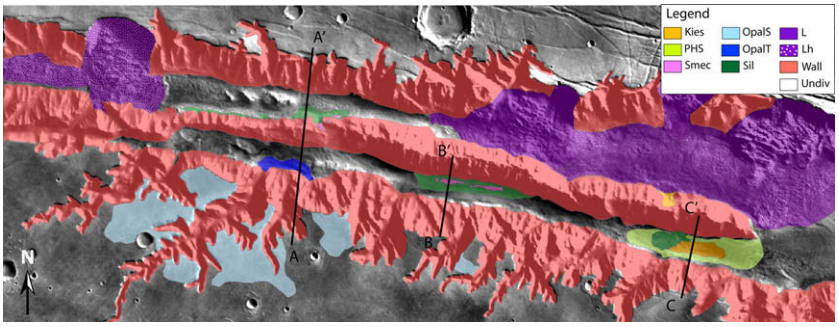

Fig. 5. Regional geologic map of Ius Chasma. Unit descriptions in Table 2, from spectral analysis of targeted CRISM observations and morphologic contact mapping of CTX and HiRISE data. Kies: kieserite, PHS: polyhydrated sulfate, Smec: Fe/Mg smectite, OpalS: sedimentary opal, OpalT: transported opal, Sil: massive hydrated silicate, L: landslide, Lh: landslide with hydrated mineralogy, Wall: wallrock, Undiv: undivided floor units. Locations of three cross-sections (Figs. 6 and 8) are labeled.

hydrated silicate units. Layered sedimentary Fe/Mg smectite clays comprise the lowest exposed stratigraphy in the central region of Ius Chasma. The layers dip at the same angle as the current surface, ~10°. The Fe/Mg smectite layers are eroded and unconformably overlain by the massive hydrated silicate unit (Fig. 9). These units are best exposed on the north side of southern Ius Chasma. A thin opal-bearing deposit overlays both of these units at the base of Louros Valles, on the southern side of the chasma.

Cross-section C–C′ (Fig. 8B) shows sulfates in the lowest region within Ius Chasma, in an enclosed basin in the easternmost part of the trough (Fig. 10). Kieserite is found at elevations less than −4175 m and corresponds to a closed basin. Polyhydrated sulfate

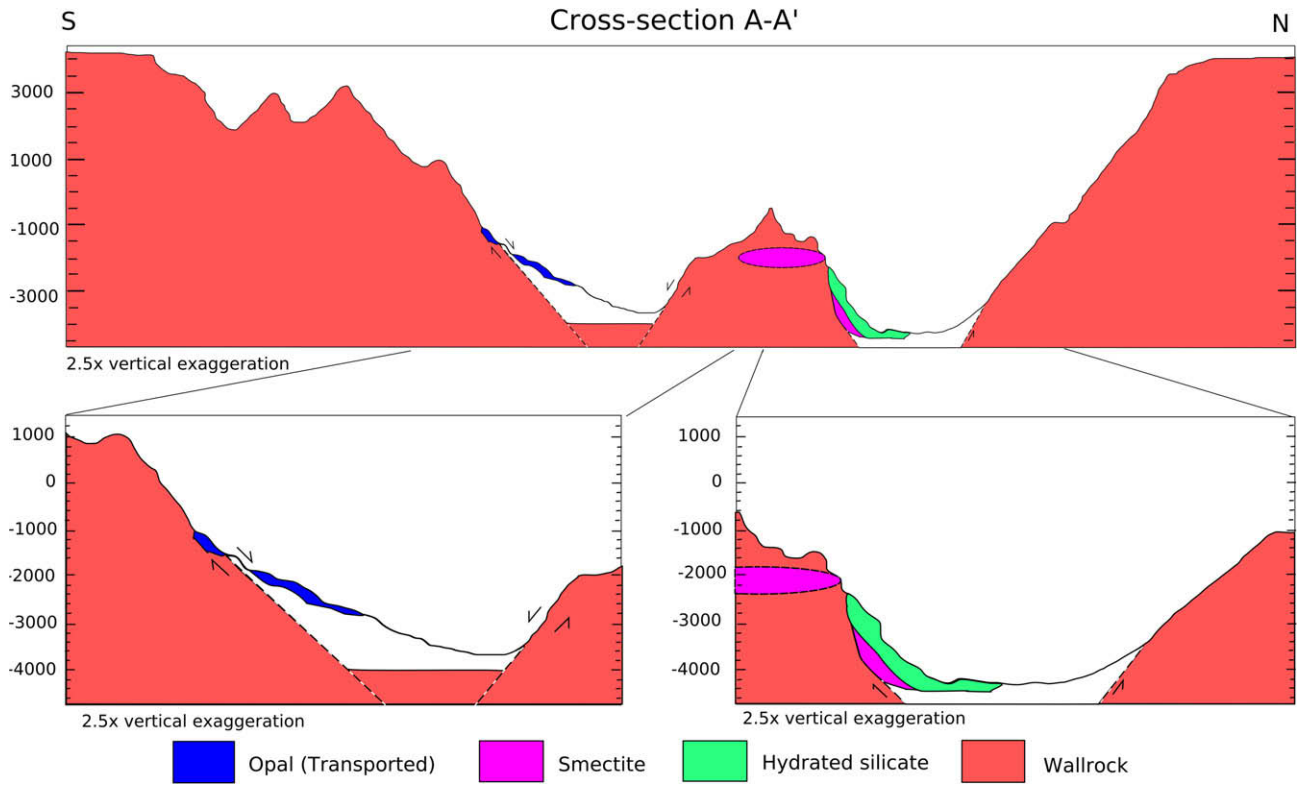

Fig. 6. Cross-section A–A′ covering opal at base of sapping channels and hydrated silicate unit overlaying layered smectite clay unit on chasma floor. Arrow indicates location of Fig. 3B. Colors of geologic units same as Fig. 5. (For interpretation of the references to colour in this figure legend, the reader is referred to the web version of this article.)

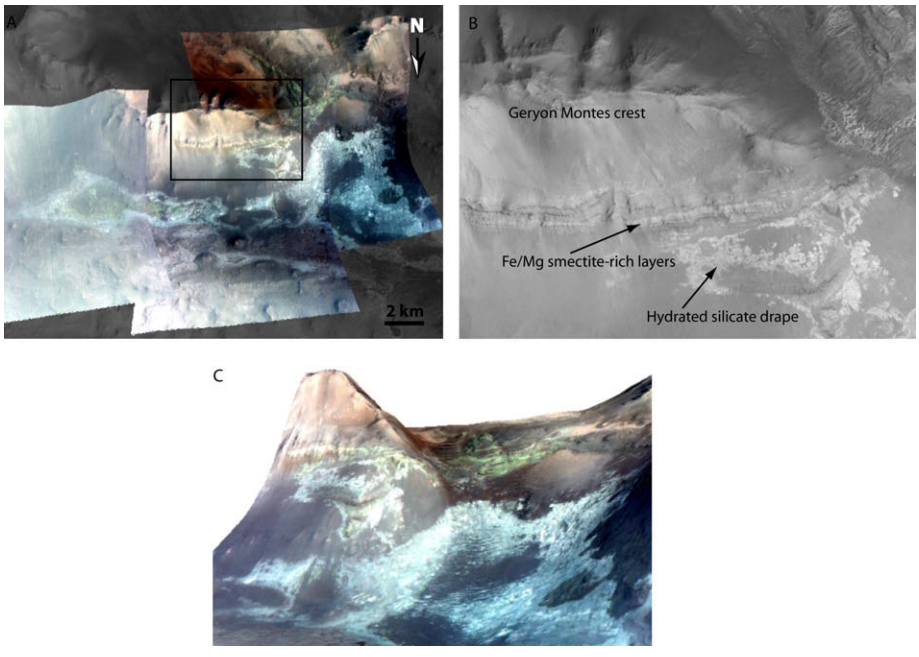

Fig. 7. Fe/Mg smectite-rich layers in Geryon Montes wallrock. (A) CRISM false color (RGB: 2.5, 1.5, 1.08 μm) over CTX mosaic. Fe/Mg smectite-rich materials in the wallrock and redeposited on the chasma floor appear greenish and hydrated silicate-rich materials draping the deposits are bluish. Black box in location of panel B. North is down. (B) CTX P16_007430_1727 showing continuity of layering in Fe/Mg smectite-rich bedrock, traceable around Geryon Montes. North is down and sun illumination from the bottom. (C) CRISM FRT00009B27 false color draped over MOLA topography. (For interpretation of the references to colour in this figure legend, the reader is referred to the web version of this article.)

is found at higher elevations (−3700 to −4175 m) than the kieserite. While the polyhydrated sulfate occurrences lie at a roughly consistent elevation and surround the kieserite, CRISM coverage is not complete enough to resolve if they lie within a closed basin. More CRISM imagery is necessary to bracket the extents of the sulfate units. Also, there are no erosional windows through the kieserite to reveal the mineralogy of the lower rock units. Current high resolution imagery is not sufficient to resolve if the kieserite over-

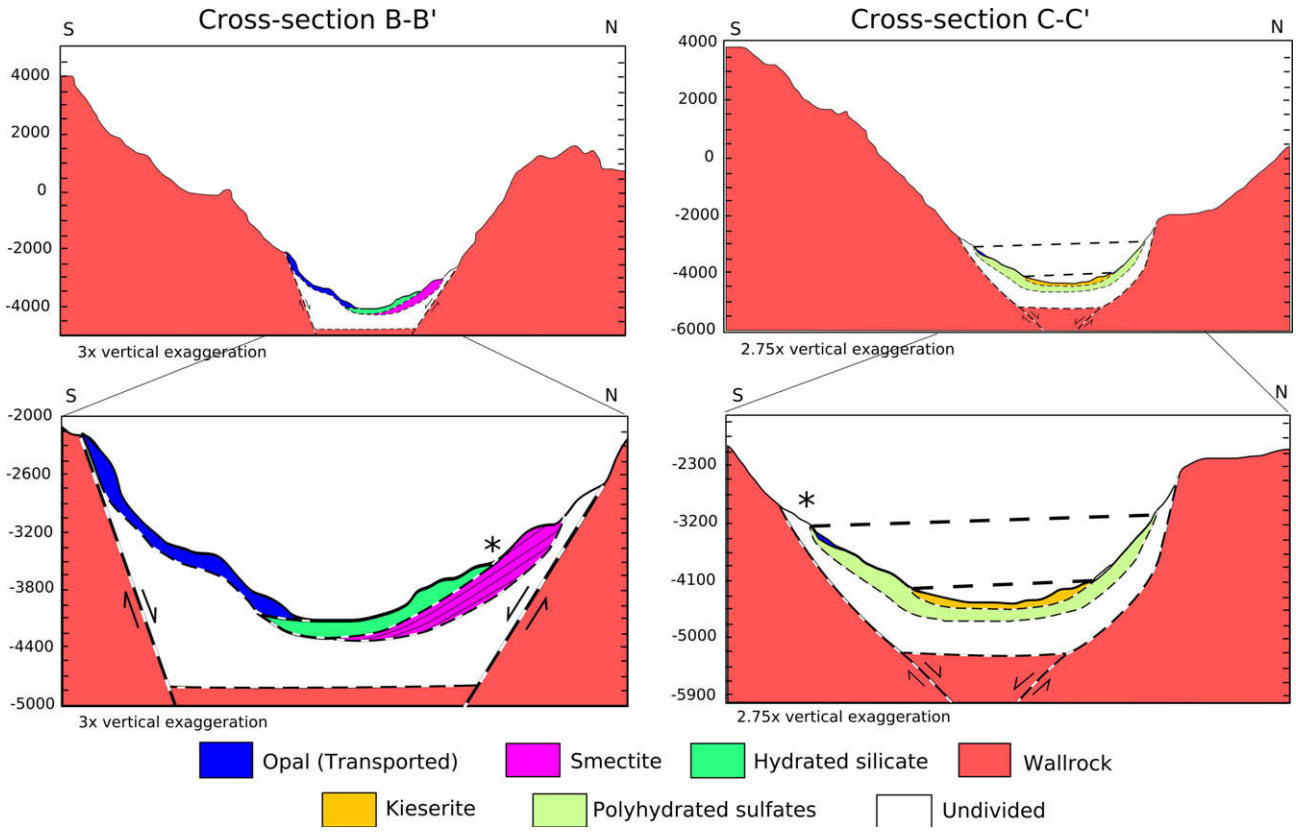

Fig. 8. (A) Cross-section B–B′ covering stratigraphic contacts of hydrated silica, hydrated silicate, and Fe/Mg smectite clay units. ∗ indicates location of Fig. 9. (B) Cross-section C–C′ detailing stratigraphy of closed evaporite basin with kieserite and polyhydrated sulfate, overlain by thin opal layer derived from the sapping channels. ∗ indicates location of Fig. 11. Colors of geologic units same as Fig. 5. (For interpretation of the references to colour in this figure legend, the reader is referred to the web version of this article.)

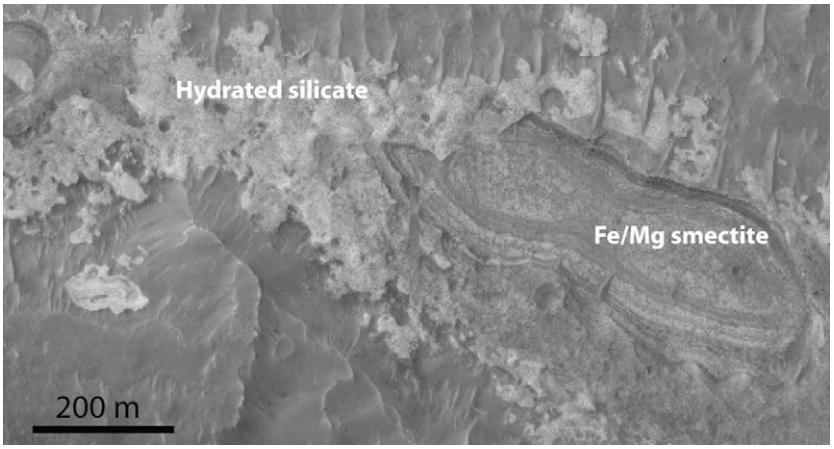

Fig. 9. Contact between layered sedimentary Fe/Mg smectite with massive hydrated silicate showing erosional unconformity (HiRISE PSP_006718_1720). Pyroxene-rich dunes and spectrally neutral capping material overlie hydrated minerals.

lies or underlies the polyhydrated sulfate. Both possible interpretations are discussed in Section 5.4. Like the layered sedimentary Fe/Mg smectite unit, there is a ~10° southerly dip to the contact between kieserite and polyhydrated sulfate. The eastern portion of the −3700 m contour which would define a closed basin for the polyhydrated sulfate is unfortunately covered by dunes and thick dust deposits, mapped as undivided floor material in this study.

Massive hydrated silicate deposits also appear over the same elevation range as the polyhydrated sulfate (not shown in Fig. 8B, but shown in Fig. 10). However, sufficient HiRISE imagery does not exist to discern the stratigraphic relationship between massive hydrated silicate and polyhydrated sulfate within Ius Chasma. At the eastern edge of the evaporite deposit, in western Melas Chasma and thus outside the scope of this study, CRISM targeted observations show a massive deposit containing hydrated silicate overlying the polyhydrated sulfate. The chasma floor between this outcrop and the mapped sulfate deposit in Ius Chasma is covered by undivided floor materials. However, we infer the relationship between massive hydrated silicate and polyhydrated sulfate to be the same in both

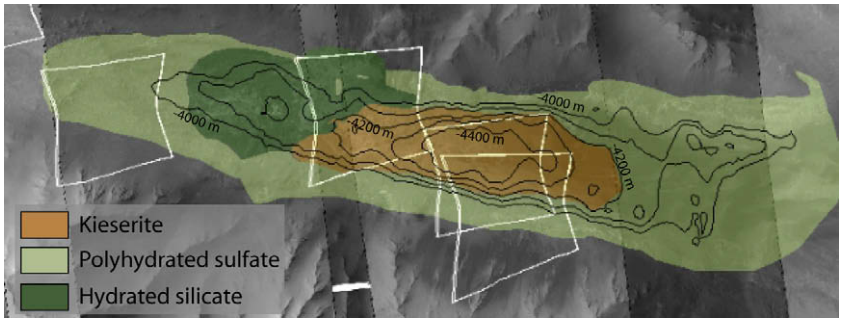

Fig. 10. Kieserite and polyhydrated sulfate deposit showing topographic restriction of kieserite as outlined in MOLA 100 m contours. White outlines of CRISM targeted observations over CTX mosaic. Kieserite (orange) is within a closed basin and polyhydrated sulfate (light green) occurs over a limited elevation range, but insufficient imagery to determine if it is within a closed contour. Hydrated silicate (dark green) overlies both. (For interpretation of the references to colour in this figure legend, the reader is referred to the web version of this article.)

chasmata, and extrapolate that the hydrated silicate probably overlies the sulfate units in Ius Chasma.

There is a slight southerly dip to the planes described by the contacts between the kieserite and polyhydrated sulfate and at the uppermost elevations of polyhydrated sulfate exposure. A very thin opal-bearing deposit overlies the evaporite deposit in the south (Fig. 11). The polyhydrated sulfate and opal have cross-cutting fractures. Like cross-section A–A′ to the west, opal is found on the plateau eroded by Louros Valles and in lobate deposits at the base of Louros Valles (Fig. 11).

Massive hydrated silicate and Fe/Mg smectite also appear in the breccia and cementing material of many, but not all landslides (Fig. 12 shows landslide with hydrated mineralogy, context shown in Fig. 1). The bluish tones in Fig. 12A are associated with hydrated mineral-rich breccia blocks and matrix, while the redder tones are associated with material that both underlies and overlies the bluish toned rocks interpreted to be unhydrated material from the same landslide. HiRISE imagery (Fig. 12B and C) shows that breccia blocks with hydrated materials are extensively folded and fractured. Hydrated materials are not seen in any of the landslide scars or in any wallrock.

5. Discussion

5.1. Mineral interpretations

There are four hypotheses for the mineral type represented by the new hydrated mineral phase identified in Ius Chasma and elsewhere in Valles Marineris: (1) sulfates structurally similar to gypsum or jarosite, perhaps in a mixture, (2) opal mixed with Fe/Mg smectite, possibly as a result of acid leaching of smectite, (3) a combination of Al- and Fe/Mg-bearing smectites, and (4) poorly crystalline mixed Al-ferric clay formed from acid alteration of Fe/Al smectite clay.

Gypsum- or jarosite-group sulfates are close matches to the new hydrated mineral phase, but their multiple absorptions in the 2.2 μm region do not perfectly correspond. Cloutis et al. (2006) attributes the 2.21–2.26 μm doublet in jarosites to a combination of OH stretch and OH out-of-plane bend, and the 2.25–2.265 μm doublet in gypsum to OH combinations. Jarosites have infinite sheet structures and gypsum has alternating chains of edge-sharing SO_4 tetrahedra and polyhedra (Hawthorne et al., 2000), so other sulfates with similar structures would be the most likely candidates to have a doublet near 2.21 and 2.27 μm. Other Ca-sulfates such as bassanite and anhydrite are structurally similar to gypsum, but neither matches spectrally. Bassanite has absorptions at 1.42 and 1.91 μm, a shoulder at 2.25 μm, and a drop of longward of ~2.4 μm (Crowley, 1991). Anhydrite has no absorptions in the VNIR since it lacks hydroxyls and H_2O in this structure. Na, K, and H_3O-bearing jarosites do not match exactly and more exotic jarosites (e.g. Ag and Pb) are geologically unlikely. The doublet in K-jarosite is significantly deeper at 2.267 than at 2.21 μm, natrojarosite has a single absorption at 2.267, and hydronium jarosite has an absorption near 2.25 μm (Bishop and Murad, 2005; Swayze et al., 2008a).

Opal has a broad absorption with a minimum at 2.21 μm due to Si-OH (silanol) groups and a shoulder at 2.26 μm, depending on how much H_2O is attached to the silanol groups (Milliken et al., 2008). However, the shape of the two features seen in the CRISM spectra is different from the bands observed in opal. Also the relative strengths of the two bands in the CRISM spectra can vary, whereas the 2.21 μm band is always stronger than the 2.26 μm band in opal. It is plausible that admixture with a smectite clay

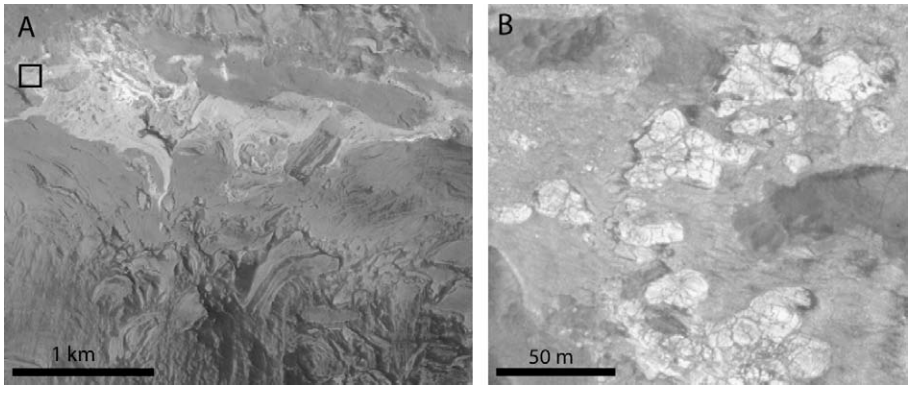

Fig. 11. HiRISE image PSP_005940_1710. (A) Lobate morphology of opal (intermediate toned) and non-hydrated dark material at base of Louros Chasma. Box indicates location of B. (B) Polyhydrated sulfate (brighter) and opal (intermediate) units have cross-cutting fractures. Opal overlies polyhydrated sulfate in thin layer. Overlain by loose, non-hydrated dark material thin enough to only partially fill fractures.

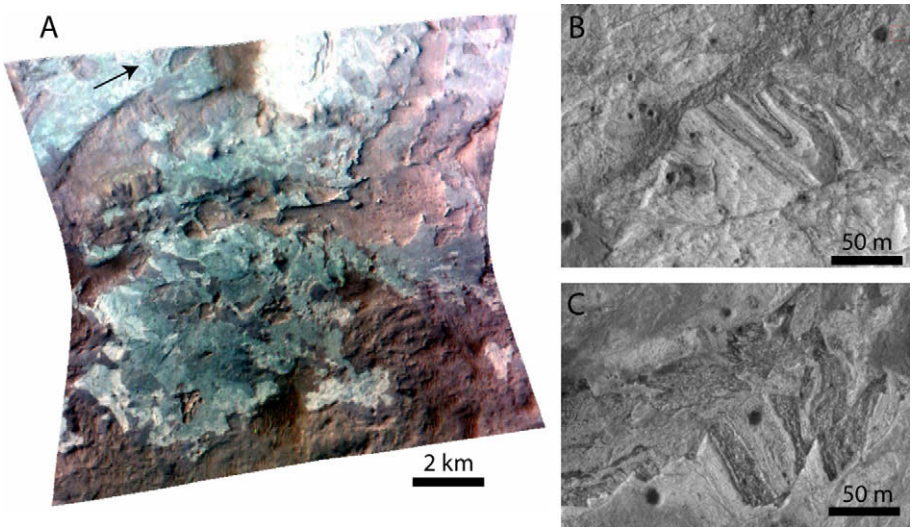

Fig. 12. (A) CRISM FRT0000A396 false color (RGB: 2.5, 1.5, 1.08 μm) of hydrated silicate material (bluish tones) and non-hydrated material (reddish tones) in landslide on Ius Chasma floor, both in breccia blocks and cementing material. Arrow points to location of (B) and (C), subsets of HiRISE PSP_006652_1725. Both show folds, fractures, and megabreccia blocks. (For interpretation of colour mentioned in this figure, the reader is referred to the web version of this article.)

such as nontronite with its 2.28 μm minimum could recreate the 2.21–2.27 μm doublet. However, the Si-OH bands in opal are broader than the metal-OH bands in phyllosilicates, and the doublet in CRISM spectra is too narrow to be fit by a large component of hydrated silica.

A mixture of smectite clays could produce overlapping narrow absorptions in the 2.2 μm region that reproduce the 2.21–2.27 μm doublet in the CRISM spectra – ferromagnesian smectites have a range of Fe/Mg overtones at 2.28–2.31 μm and montmorillonite as an Al-OH overtone at 2.21 μm. The variable relative band depths in the CRISM spectra are consistent with a mixture of varying composition. Both montmorillonite and Fe-rich smectite have been found in separate deposits elsewhere on Mars (e.g. Poulet et al., 2005; Mustard et al., 2008; Wray et al., 2008a), and Al-rich phyllosilicate is found above Fe/Mg smectite in wallrock in Coprates Chasm (Murchie et al., 2009a). An intimate mixture of jarosite and montmorillonite would have a similar spectral shape to a mixture of Fe-rich smectite and montmorillonite. Its doublet would be at 2.20–2.21 and 2.267 μm, which is a close match, but still does not fully explain the range in the position of the longer absorption. Jarosite forms at pH < 3, so this mixture would indicate very acidic conditions (Bigham et al., 1996).

The last hypothesis is an poorly crystalline Fe–SiO_2 phase due to either (1) acid leaching of a smectite or (2) neoformation from dissolved basaltic material. Neutral- to acidic-leaching of aluminous nontronite reduces the intensity of the 2.23 and 2.29 μm absorptions and creates a broader absorption at 2.20–2.22 μm due to silanol vibrations from the formation of amorphous silica (Madejova et al., 2008). Fig. 4B shows an example of Fe/Mg smectite-rich material on Mauna Kea that was leached by acidic vapors or fluids (G. Swayze, unpublished data). The material has a broad absorption at 2.20 μm due to amorphous silica as well as a 2.29 μm band, due to FeFeOH bend and stretch combinations, and a 2.23 μm band, due to FeAlOH vibrations (Frost et al. 2002). The absorptions vary in strength, probably depending on the degree of acid alteration.

A second type of poorly crystalline Fe–SiO_2 phase is neoformed in a laboratory under oxidizing conditions and pH 8. Laboratory studies of smectite or silicate neoformation from solutions approximating dissolved martian basalt with additions of S and Cl (Tosca et al., 2008) have produced an XRD amorphous phase with a possible doublet at 2.21 and 2.27 μm. It is described as a poorly crystalline Fe–SiO_2 bearing precipitate. The phases present as a result of $FeSiO_2$ interactions can depend on the pH and Fe oxidation state (Pokrovski et al., 2003). Its continuum-removed spectrum matches the CRISM spectra (Fig. 4C) and suggests that precipitation of material by dissolution of basalt and addition of S and Cl under circumneutral pH conditions could replicate the new hydrated phase. Two different formation processes – transformation and neoformation – can both produce Fe–SiO_2-bearing phases that straddle the boundary between sulfates and smectites. Together, the poorly crystalline Fe–SiO_2 phases offer plausible models for the hydrated silicate phase.

Of the four possible mineralogies of the hydrated mineral phase, we favor three: a neutral- to acid-neoformed $FeSiO_2$ phase or leached phyllosilicate, a montmorillonite/jarosite mixture, or a montmorillonite/ferromagnesian smectite mixture. While none are perfect spectral matches, all are geologically feasible with the other alteration minerals found in Ius Chasma.

5.2. Integrating hydrated mineralogy with stratigraphy

Fitting the hydrated mineral deposits from this study into the previously proposed stratigraphy of Ius Chasma gives new insight into the intersection of its aqueous and structural history. Previous morphologic and structural mapping efforts (Tanaka, 1986; Lucchitta and Bertolini, 1989; Lucchitta et al., 1992; Peulvast and Masson, 1993a,b; Peulvast et al., 2001), combined with the mineralogic results presented in this paper, reveal the following updated geologic history:

1. Formation of the early Noachian basement.
2. Partial alteration of basement to Fe/Mg smectite.
3. Late Noachian to Hesperian lava flows over the basement/regolith create several km of layered basalts.
4. Valles Marineris forms by repeated tectonic extension in late Hesperian, forming horst and grabens in Ius Chasma. Erosion creates spur-and-gully morphology on wallrock. Both Hesperian and Noachian materials may be exposed in wallrock.
5. Continuous mass wasting transports altered wallrock rich in Fe/Mg smectite into Ius Chasma as sedimentary fines and breccia blocks. Fines accumulate into layered deposits on chasma floor.
6. The layered sedimentary Fe/Mg smectite is eroded by fluvial or aeolian processes.

7. Surface water geochemistry changes to more acidic conditions, and sulfate precipitates from evaporating brines at the lowest elevations.
8. Hydrated silicate is deposited as massive layer on top of layered sedimentary Fe/Mg smectite and sulfate deposits and as matrix material cementing (altered) megabreccia.
9. The uppermost layer of basaltic wallrock is altered to opal-bearing material.
10. Fluvial processes along Louros Valles bring opal into Ius Chasma as sedimentary particles or precipitates. Louros Valles may predate transport of opal-bearing materials. Louros Valles morphology controlled by fractures related to Valles Marineris or to older Noachian stresses.
11. "Recent" tectonism cuts Louros Valles and possibly widens connection between Ius and Melas Chasmata. Differential slip along southern walls tilts the chasma floor.
12. Landslides without hydrated material partially cover landslides containing hydrated silicate.

From this geologic history, we interpret the aqueous geochemistry to be first neutral-to-alkaline, resulting in alteration of crustal material to Fe/Mg smectite; then neutral to very acidic, resulting in sulfate precipitation and and possibly alteration of smectite or precipitation of basaltic precursor material as a poorly crystalline $FeSiO_2$ phase or jarosite/smectite mixture; and then very acidic, resulting in spatially extensive precipitation of opal on the plateau (Fig. 13). This opal co-occurs with a dehydrated jarosite elsewhere on the plateau surrounding Valles Marineris, indicating low pH conditions (Milliken et al., 2008; Weitz et al., 2008). Jarosite forms most commonly under low temperature, low pH (<4) conditions (Stoffregen et al., 2000). While jarosite has not been found with the opal on the plateau south of Ius Chasma, we interpret the presence of sedimentary opal as indicative of acidic geochemistry demonstrated by the opal and jarosite mineralogy elsewhere on the plateau (Milliken et al., 2008; Weitz et al., 2008; Bishop et al., 2009). This interpreted trend in aqueous geochemistry is consistent with other OMEGA and CRISM studies suggesting widespread change in the character of aqueous mineral assemblages in late Noachian to Hesperian time, from ones consistent with a neutral or alkaline environment to ones indicating a relatively acidic and saline environment (Bibring et al., 2006; Murchie et al., 2009a). Details of the timing of that environmental transition, from phyllosilicate formation in Noachian terrains to sulfate formation in Hesperian terrains, may be captured in Ius Chasma.

5.3. Formation and transportation of Fe/Mg smectite

The Geryon Montes wallrock is altered to Fe/Mg smectite near −2000 m elevation (Fig. 7); materials at that elevation may be early Hesperian lavas or Noachian basement, although faulting may have displaced Geryon Montes upwards from its original elevation. Geryon Montes is a central horst bracketed to the north and south by graben, and stratigraphically deeper (Noachian) section may have been elevated by tectonism and exposed in the ridge. Other outcrops of Noachian-aged wallrock in Capri and Coprates Chasmata also expose Fe/Mg smectite-rich layers (Murchie et al., 2009a). Fe/Mg smectite or other hydrated alteration products are not found in the bulk of the Hesperian-aged lava flows; the upper, Hesperian-aged wallrock and many landslides sourced from there do not exhibit a signature of hydrated or hydroxylated phases. The opal detected on the uppermost surface of the Hesperian lava flows probably correspond to acidic surface alteration rather than to older crustal alteration that formed the smectite clays.

The opal-bearing deposits in the chasma floor have an overlapping, lobate morphology consistent with viscous flow. The opal-bearing floor deposits could have formed one of two ways: (1) opal was transported into southern Ius as a thin deposit that thins to less than the detection limit further away from Louros Valles, and (2) unaltered material travelled into Ius Chasma along Louros Valles and was subsequently altered to opal by similar processes that formed the opal on the plateau.

The tectonism, mass wasting, and fluvial erosion associated with the opening of Ius Chasma is expected to have mobilized Fe/Mg smectite-rich fines and redeposited them in sedimentary materials on the trough floor. Layered, sedimentary Fe/Mg smectite is visible in the western and both the northern and southern subbasins of central Ius, but are not exposed in eastern Ius. The stratigraphic relationship between the sulfates and smectite units is unclear – the layered smectite deposits may be covered by later sulfate evaporites or they may postdate the sulfates. The layered sedimentary smectites are also themselves eroded by subsequent fluvial or aeolian processes. They may have been emplaced as a drape or been originally flat-lying but tilted down to the south during late stage normal faulting that occurred preferentially on the southern part of the graben (Peulvast and Masson, 1993a).

5.4. Evidence for sulfate evaporites in a paleobasin

Kieserite and polyhydrated sulfate are both found within a closed topographic basin in eastern Ius Chasma. The polyhydrated sulfate is found at higher elevations, and kieserite at lower elevations, and the deposits together span ~700 m in elevation. This sulfate deposit in a local depression is unlike any other sulfate deposit in Valles Marineris. The ~10° northerly dip of these sulfate units may be due to late-stage preferential faulting on the southern part of graben(s) underlying the southern Ius Chasma floor, as is suggested above for the hydrated deposits in Cross-section B–B′. Elsewhere in Valles Marineris, sulfate is found in mound-shaped,

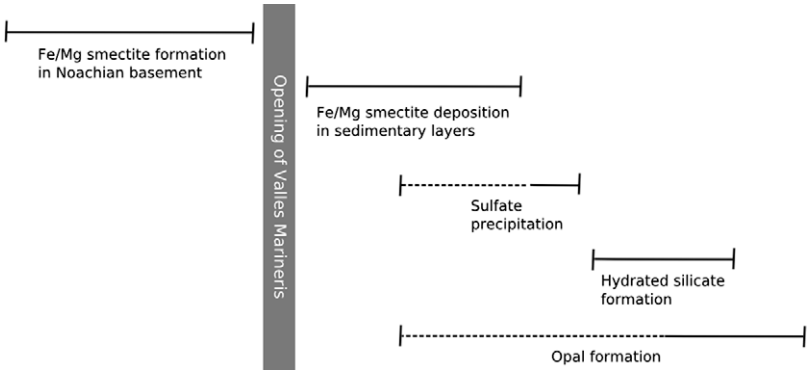

Fig. 13. Relative timeline of hydration mineral formation in Ius Chasma, Valles Marineris.

friable, layered deposits that can reach several km in thickness (e.g. Gendrin et al., 2005). There are several hypotheses for how distinct monohydrated and polyhydrated sulfates formed in those areas: by sequential deposition in an evaporating basin, through dehydration of a polyhydrated Mg sulfate to kieserite by heating after burial, or through dehydration of an existing polyhydrated sulfate deposit by upwelling, hydrophillic chloride-rich brines within a tectonically active fault basin (as in Hardie, 1991). We will briefly discuss each one and point out questions that remain.

The elevation distribution of the sulfate phases is consistent with concentration of an evaporating brine that first precipitated polyhydrated phases and then precipitated monohydrated sulfates at the near-terminal stage of evaporation (Spenser, 2000). The sulfate deposits are thin enough that they would conform to the pre-existing basin topography rather than completely fill the basin. Thus, the kieserite is stratigraphically higher than the polyhydrated sulfate even though it is exposed at lower elevations (Fig. 8). Ius Chasma may have been somewhat isolated from Melas Chasma at that time, which would make it easier for water to pond and evaporate. However, there are several uncertain aspects of the evaporite model. First, if the kieserite is from terminal evaporation of a brine and kieserite is exposed over 200 m, that implies a relatively large volume of water for an end stage evaporite mineral. Second, the polyhydrated sulfate unit beneath the kieserite unit is not exposed in erosional windows, so the continuity of the polyhydrated sulfate unit is uncertain. Thus, while an evaporite basin is consistent with regional topography and mineral stratigraphy, the hypothesis would be greatly strengthened if it could be shown that the polyhydrated sulfate underlies the kieserite.

The second hypothesis is that the kieserite is a diagenetic phase formed from polyhydrated Mg sulfate. The bulk of the sulfate detected in Valles Marineris is within light-toned, layered deposits that range in size from tens to hundreds kilometers wide and hundreds meters to 4 km thick (Gendrin et al., 2005; Bishop et al., 2009; Murchie et al., 2009b; Roach et al., 2009). Kieserite units are typically found beneath polyhydrated sulfate-rich units, especially in large deposits several kilometers in thickness, and may be diagenetic products formed by dehydration of polyhydrated Mg sulfates, like epsomite ($MgSO_4{\cdot}7H_2O$) (Roach et al., 2009). This diagenesis requires burial to a few km to reach high enough temperatures for sulfate conversion (Roach et al., 2009). The deposit in Ius Chasma is too thin to have converted to kieserite via diagenesis, barring a very localized, unusually high geothermal gradient beneath the basin, such as by buried insulating salts (Kargel et al., 2007), or the influx of hydrophilic brines. Active grabens often have low water activity hydrothermal brines (Hardie, 1983), which can dehydrate epsomite to kieserite (Hardie, 1991).

The third hypothesis also involves conversion of a sulfate sequence to Mg-rich sulfates, like kieserite, and includes aspects of both previous hypotheses. The sulfate is originally precipitated as an evaporite in an extensional fault basin. Hydrophilic brines produced hydrothermally during periods of tectonic or magmatic activity upwell and percolate through the sulfates (Hardie, 1991). The brines have a low water activity and readily convert polyhydrated sulfates to kieserite. Perhaps the upwelling brines only permeated the lower 400 m of exposed sulfates, such that the overlying polyhydrated sulfates remained unaltered. This hypothesis is a controversial hypothesis used to explain massive Mg sulfate-rich evaporite deposits on Earth, and the implications for its application to a martian evaporite sequence (i.e. Tosca and McLennan, 2006) are not yet worked out.

We consider the evaporite basin with successive draped layers of sulfates as the parent brine concentrated to be the most feasible interpretation, but the relative importance of low temperature diagenesis and later low water activity brine recirculation is unknown.

5.5. Relationships between smectites, sulfates, and hydrated silicate

Fe/Mg smectite clays and sulfate are not found together in any CRISM image of Valles Marineris. The location of the expected contact between the two units in central Ius Chasma has not yet been imaged with CRISM, but CTX images suggest that the contact would be obscured by mafic mineral-rich dunes and other mobile material. However, the relative timing of the sulfate deposition and the unconformity between Fe/Mg smectite and massive hydrated silicate can be partially constrained. The Fe/Mg smectite clays were deposited, then eroded, then capped by hydrated silicate. The sulfate evaporite sequence is capped by the same massive hydrated silicate unit, so the sulfates must have formed before the clay minerals were covered by the hydrated silicate.

The contact between the finely layered sedimentary Fe/Mg smectite and the massive hydrated silicate marks a change in regional aqueous geochemistry to more acidic conditions. Neutral to acidic surface water or groundwater would have partially leached Fe/Mg smectite fines, which were then deposited over the length of Ius Chasma, in a few meter-thick layer and as matrix material within landslides. Alternatively, very acidic surface water could have partially dissolved smectite materials and precipitated a few meter-thick layer of jarosite-cemented smectite particles. A third option is that the hydrated silicate is a multiple smectite mixture (containing Al, Mg, and Fe cations) perhaps formed by further alteration of the Noachian-aged Fe/Mg smectite. Landslides with hydrated minerals have Fe/Mg smectite and hydrated silicate in both matrix material and the megabreccia blocks. The Fe/Mg smectite-bearing megabreccia from Noachian wallrock was likely deposited on the trough floor by landslides. More recent landslides sourced from dominantly Hesperian wallrock do not show hydrated mineralogy, consistent with the model of decreasing water availability with time (Jakosky and Phillips, 2001).

Several relationships between the hydrated silicate material and other minerals can help constrain the relative stratigraphy. First, the hydrated silicate material is found in three types of locations within Ius Chasma: in landslides from the wallrock, unconformably overlying layered Fe/Mg smectite clays, and overlying sulfates. It is found in both the breccia and cementing material of many, but not all landslides. Landslides may contain both hydrated, Noachian-aged material and non-hydrated, Hesperian-aged material. Second, smectite clays are found in several places within the chasma in deposits that appear finely layered at HiRISE resolution, and they are unconformably overlain by the hydrated silicate material (Fig. 9). The hydrated silicate material does not show layering and has an apparent thickness of a few meters. Third, in the sulfate deposit at the eastern end of Ius Chasma, the hydrated silicate is found at a higher elevation than kieserite and over the same range in elevations as the polyhydrated sulfate. Further east in Melas Chasma, the eastern edge of the polyhydrated sulfate unit in the evaporite deposit is overlain by hydrated silicate. HIRISE imagery shows the hydrated silicate has a lobate, hummocky morphology, which previous studies have suggested is caused by landslide movement (Weitz et al., 2003; Pelkey et al., 2003).

The stratigraphic relations between hydrated mineralogies can also help us resolve the relative timing of aqueous alteration and the last tectonic activity. The opal deposits are found at the base of Louros Valles sapping channels, but not in northern Ius Chasma which has less prevalent sapping morphology. If the opal-bearing material was transported onto the chasma floor as particles or dissolved precipitates by the groundwater sapping that formed Louros Valles, then the opal would be most concentrated close to the source. The thin opal-bearing deposit superposes a polyhydrated sulfate unit. Thus the latest sapping event(s) are posited to postdate the evaporation of the closed sulfate-rich basin. Nearby, opal-rich material at the bottom of a sapping channel is cut by a

basal scarp formed by late tectonic activity. Since opal is the last of the hydrated alteration materials to be emplaced in Ius Chasma, this suggests that deposition of alteration phases occurred before the most "recent" tectonism, such as the southerly slip of the southern Ius Chasma graben(s). The "recent" tectonism, as described by Peulvast and Masson (1993a,b), cannot be precisely dated, but it postdates deposition of all hydrated phases and much of the mass wasting activity in Ius Chasma.

6. Conclusions

The superposition of different hydrated phases and the different morphologies of units containing them suggest a series of several distinct aqueous events in Ius Chasma. In the central region, Fe/Mg smectite clays are found in finely layered deposits, which favors a transportation and deposition model rather than *in situ* alteration. Subsequent erosion of the Fe/Mg smectite and their unconformable superposition by massive hydrated silicate points to multiple fluvial events sculpting the floor of Ius Chasma. If the hydrated silicate material is a poorly crystalline Fe–SiO_2 phase, then its presence indicates a change from alkaline to more neutral or acidic surface- or groundwater. In this scenario, either (1) acidic surface or ground water partially altered the Fe/Mg smectite clay to a less crystalline, leached smectite, which was deposited in a thin layer along Ius Chasma, or (2) more acidic groundwater promoted neoformation of poorly crystalline Fe–SiO_2 phases from basaltic weathering products. If the hydrated silicate material is instead a jarosite/smectite mixture, it indicates an aqueous environment with pH < 3, where partial smectite dissolution is followed by precipitation of jarosite as a cement for Al-rich smectite. Fe/Mg smectite-bearing breccia blocks in landslide deposits on the floor of Ius were also partially altered to hydrated silicate. If the hydrated silicate in the landslide deposits was a mixture of smectite clays, then either the Fe/Mg smectite further altered to a new smectite mixture, or the Noachian-aged material contains multiple domains of smectite alteration. Deposition of opal-bearing material by sapping channels was a late stage event which overlaid the sulfate sequence to the east. The alteration to opal might also have happened after the material was transported into the chasma. Similar aqueous activity was reported in western Candor Chasma, where fluvial erosion and redeposition of sulfates following formation of sulfate-bearing deposits (Murchie et al., 2009b). Perhaps fluvial activity persisted for a significant time after sulfate deposition and after erosion of the sulfate host material in both Ius and Candor Chasma. Tectonic activity continued after the last hydrated minerals were formed, as seen in the normal faulting on the southern walls that cut all hydrated mineral outcrops.

The hydrated silicate found throughout Valles Marineris could indicate a complex smectite mineral assemblage, acidic alteration of crustal phyllosilicate, or near neutral precipitation of basaltic weathering products. Regardless of the exact mineralogy of the hydrated silicate, this material is a marker for "intermediate" conditions in between the neutral-to-alkaline smectite units and the acidic opal-jarosite plateau deposits. Fe/Mg smectites have been found in Noachian-aged crust throughout Mars (Mustard et al., 2008), but the hydrated silicate is restricted to Valles Marineris. If Mars did undergo a global transition from alkaline to acidic conditions, then similar and/or additional "intermediate" mineralogies should be expected where phyllosilicate- and mafic-bearing Noachian crust was in contact with acidic groundwater to an extended period of time. Global hydrologic modeling has shown Valles Marineris, its outflow channels, and Meridiani Planum to be locations of sustained upwelling that would have supported the deposition of large volumes of acidic minerals (Andrews-Hanna et al., 2007; Murchie et al., 2009b). However, several large highland craters outside these locations (Columbus, Cross, Gale, and Schiaparelli craters) also host significant sulfates (Wray et al., 2008b; Swayze et al., 2008b; Milliken et al., 2009; Wiseman et al., 2009). The transition from alkaline to more acidic groundwater was temporal and may be widespread in location than current detections suggest.

The stratigraphy and hydrated mineralogy in Ius Chasma both argue for several distinct phases of erosion and aqueous processes. The environmental progression from alkaline/neutral to acidic conditions with time could be caused by several mechanisms. Increased volcanism outgassing more H_2S combined with decreased water activity or availability due to crustal cooling could be one way to acidify groundwater and change the balance from phyllosilicate to sulfate precipitation (e.g. Pollack et al., 1987).

Ius Chasma is a superb location for future landed missions as it has extensive expression of a diversity of hydrated alteration minerals, shows a variety of geologic processes – volcanic, tectonic, and fluvial, and contains excellent exposures of Hesperian and Noachian-aged materials. It is an ideal location to study the transition in global aqueous geochemistry in the mineralogy, morphology, and geologic relationships of a collection of diverse hydrated minerals.

Acknowledgments

We are grateful to Jim Crowley and Dave Bish for helpful discussions about spectral identification of the hydrated silicate and thank Nick Tosca for graciously sharing preliminary experimental results. We thank Tim Glotch and Nick Tosca for reviews which significantly improved the manuscript. We appreciate the contributions of the CRISM team, and especially thank the entire CRISM SOC for running such a successful mission!

References

Anderson, J.H., Wickersheim, K.A., 1964. Near infrared characterization of water and hydroxyl groups on silica surfaces. Surf. Sci. 2, 252–260.
Andrews-Hanna, J., Phillips, R., Zuber, M., 2007. Meridiani Planum and the global hydrology of Mars. Nature 446, 163–168. doi:10.1038/nature05594.
Bibring, J.-P., and 10 colleagues, 2006. Global mineralogical and aqueous Mars history derived from OMEGA/Mars express data. Science 312, 400–404.
Bibring, J.-P., and 11 colleagues, 2007. Coupled ferric oxides and sulfates on the martian surface. Science 317, 1206–1210.
Bigham, J.M., Schwertmann, U., Pfab, G., 1996. Influence of pH on mineral speciation in a bioreactor simulating acid mine drainage. Appl. Geochem. 11, 845–849.
Bishop, J.L., Pieters, C.M., Green, J.O., 1994. Infrared spectroscopic analysis on the nature of water in montmorillonite. Clays Clay Miner. 42 (6), 702–716.
Bishop, J.L., Murad, E., 2005. The visible and infrared spectral properties of jarosite and alunite. Am. Mineral. 90, 1100–1107.
Bishop, J.L., Lane, M.D., Dyar, M.D., Brown, A.J., 2008. Reflectance and emission spectroscopy study of four groups of phyllosilicates: Smectites, kaolinite–serpentines, chlorites and mica. Clay Mineral. 43, 35–54.
Bishop, J.L., and 12 colleagues, 2009. Mineralogy of Juventae Chasma: Sulfates in the light-toned mounds, mafic minerals in the bedrock, and hydrated silica and hydroxylated ferric sulfate on the plateau. J. Geophys. Res. doi:10.1029/2009JE003352.
Blasius, K.R., Cutts, J.A., Guest, J.E., Masursky, H., 1977. Geology of the Valles Marineris: First analysis of imaging from the Viking I Orbiter primary mission. J. Geophys. Res. 82 (28), 4067–4091.
Burns, R.G., 1993. Origin of electronic spectra of minerals in the visible to near-infrared region. In: Pieters, C.M., Englert, P.A.J. (Eds.), Remote Geochemical Analysis: Elemental and Mineralogical Composition. Cambridge Univ. Press, New York, pp. 3–29.
Carr, M.K., 1974. Tectonism and volcanism of the Tharsis region of Mars. J. Geophys. Res. 79, 3943–3949.
Christensen, P.R., and 25 colleagues, 2001. Mars Global Surveyor Thermal Emission Spectrometer experiment: Investigation description and surface science results. J. Geophys. Res. 106 (E10), 23823–23871.
Christensen, P.R., and 18 colleagues, 2003. Morphology and composition of the surface of Mars: Mars Odyssey THEMIS results. Science 300, 2056–2061. doi:10.1126/science1080885.
Christensen P.R., and 11 colleagues, 2005. Evidence for magmatic evolution and diversity on Mars from infrared observations. Nature. doi:10.1038/nature03639.

Clark, R.N., King, T.V.V., Klejwa, M., Swayze, G.A., Vergo, N., 1990. High resolution reflectance spectroscopy of minerals. J. Geophys. Res. 95 (B8), 12653–12680.
Clark, R., Swayze, N.G.A., Wise, R., Livo, K.E., Hoefen, T.M., Kokaly, R.F., Sutley, S.J., 2007. USGS Digital Spectral Library splib06a. US Geol. Surv., Data Series 231, Available from: <http://speclab.cr.usgs.gov/spectral.lib06>.
Cloutis, E., and 11 colleagues, 2006. Detection and discrimination of sulfate minerals using reflectance spectroscopy. Icarus 184, 121–157.
Craddock, R.A., Howard, A.D., 2002. The case for rainfall on a warm, wet early Mars. J. Geophys. Res. 107, 5111. doi:10.1029/2001JE001505.
Croft, S.K., 1989. Mars' canyon systems: Problems of origin. In: 4th Int. Conf. on Mars, Tucson, pp. 88–89 (abstract).
Crowley, J.K., 1991. Visible and near-infrared (0.4–2.5 μm) reflectance spectra of playa evaporite minerals. J. Geophys. Res. 96, 16231–16240.
Crowley, J.K., Williams, D.E., Hammarstrom, J.M., Piatak, N., Chou, I.-M., Mars, J.C., 2003. Spectral reflectance properties (0.4–2.5 μm) of secondary Fe-oxide, Fe-hydroxide, and Fe–sulphate–hydrate minerals associated with sulphide-bearing mine wastes. Geochem. Explorat. Environ. Anal. 3, 219–228.
Ellis, M.A., Densmore, A.L., Anderson, R.S., 1999. Development of mountainous topography in the Basin Ranges, USA. Basin Res. 11 (1), 21–41.
Ernst, R.E., Grosfils, E.B., Mege, D., 2001. Giant dike swarms: Earth, Venus and Mars. Ann. Rev. Earth Planet. Sci. 29, 489–534.
Frost, R., Kloprogge, J., Ding, Z., 2002. Near-infrared spectroscopic study of nontronites and ferruginous smectites. Spectrochimica Acta Part A 58, 1657–1668.
Gates, W.P., 2005. Infrared spectroscopy and the chemistry of dioctahedral smectites. In: Kloprogge, J.T. (Ed.), The Application of Vibrational Spectroscopy to Clay Minerals and Layered Double Hydroxides. Clay Minerals Soc., Aurora, CO, pp. 125–168.
Hawthorne, F.C., Krivovichev, S.V., Burns, P.C., 2000. The crystal chemistry of sulfate minerals. In: Alpers, C.N., Jambor, J.L., Nordstrom, D.K. (Eds.), Sulfate Minerals: Crystallography, Geochemistry, and Environmental Significance, Reviews in Mineralogy, vol. 40. Mineral. Soc. Am., Washington, DC, pp. 1–112.
Gendrin, A., and 10 colleagues, 2005. Sulfates in martian layered terrains: The OMEGA/Mars express view. Science 307(5715), 1587–1591.
Goryniuk, M.C., Rivard, B.A., Jones, B., 2004. The reflectance spectra of opal-A (0.5–25 μm) from the Taupo Volcanic Zone: Spectra that may identify hydrothermal systems on planetary surfaces. Geophys. Res. Lett. 31. doi:10.1029/2004GL021481.
Hamblin, W.K., 1976. Patterns of displacement along the Wasatch fault. Geology 4, 619–622.
Hardie, L.A., 1983. Origin of $CaCl_2$ brines by basalt–seawater interaction: Insights provided by some simple mass balance calculations. Contrib. Mineral. Petrol. 82, 205–213. doi:10.1007/BF01166615.
Hardie, L.A., 1991. On the significance of evaporites. Ann. Rev. Earth Planet. Sci. 19, 131–168.
Hunt, G.R., Salisbury, J.W., Lenhoff, C.J., 1971. Visible and near-infrared spectra of minerals and rocks – IV. Sulphides and sulfates. Mod. Geol. 3, 1–14.
Hunt, G.R., Salisbury, J.W., Lenhoff, C.J., 1973. Visible and near-infrared spectra of minerals and rocks – VI. Additional silicates. Mod. Geol. 4, 85–106.
Jakosky, B.M., Phillips, R.J., 2001. Mars' volatile and climate history. Nature 412, 237–244. doi:10.1038/35084184.
Kargel, J.S., Furfaro, R., Prieto-Ballesteros, O., Rodriguez, J., Montgomery, D., Gillespie, A., Marion, G., Wood, S., 2007. Martian hydrogeology sustained by thermally insulating gas and salt hydrates. Geology 35, 975–978. doi:10.1130/G23783A.1.
Kochel, R.C., Piper, J.F., 1986. Morphology of large Valles on Hawaii: Evidence for groundwater sapping and comparison with martian valleys. J. Geophys. Res. 91, E175–E192.
Lucchitta, B.K., Bertolini, L.M., 1989. Interior structures of Valles Marineris. Proc. Lunar Planet. Sci. Conf. XX, 590–591.
Lucchitta, B.K., Blaser, R.A., Bertolini, L.M., 1990. Valles Marineris, Mars: Are pit chains formed by erosion and troughs by tectonism. Proc. Lunar Planet. Sci. Conf. XXI, 722–723.
Lucchitta, B.K., McEwen, A., Clow, G., Geissler, P., Singer, R., Schultz, R., Squyres, S., 1992. The canyon system on Mars. In: Kieffer, H.H., Jakosky, B.M., Snyder, C.W., Matthews, M.S. (Eds.), Mars. Univ. Arizona Press, Tucson, pp. 453–492.
Lucchitta, B.K., Isbell, N.K., Howington-Kraus, A., 1994. Topography of Valles Marineris: Implications for erosional and structural history. J. Geophys. Res. 99 (E2), 3783–3798.
Madejova, J., Pentrak, M., Ralkova, H., Komadel, P., 2008. Near-infrared spectroscopy: A powerful tool in studies of acid-treated clay minerals. Vib. Spectrosc. 49 (2), 211–218. doi:10.1016/j.vibspec.2008.08.001.
Malin, M.C., and 13 colleagues, 2007. Context camera investigation on board the Mars Reconnaissance Orbiter. J. Geophys. Res. 112, E05S04. doi:10.1029/2006JE002808.
Mangold, N., Quantin, C., Ansan, V., Delacourt, C., Allemand, P., 2004. Evidence for precipitation on Mars from dendritic valleys in the Valles Marineris area. Science 305, 78–81. doi:10.1126/science.1097549.
McCauley, J.F., Carr, M., Cutts, J., Hartmann, W., Masursky, H., Milton, D., Sharp, R., Wilhelms, D., 1972. Preliminary Mariner 9 report on the geology of Mars. Icarus 17, 289–327.
McEwen, A.S., Malin, M.C., Carr, M.H., Hartmann, W.K., 1999. Voluminous Volcanism on early Mars revealed in Valles Marineris. Nature 397, 584–586.
McEwen, A.S., and 14 colleagues, 2007. Mars Reconnaissance Orbiter's High Resolution Imaging Science Experiment (HiRISE). J. Geophys. Res. 11, E05S02. doi:10.1029/2005JE002605.
McKenzie, D., Nimmo, F., 1999. The generation of martian floods by the melting of ground ice above dykes. Nature 397, 231–233.
Mege, D., Masson, Ph.L., 1996. Stress models for Tharsis formation, Mars. Planet. Space Sci. 44 (12), 1471–1497.
Milliken, R.E., and 11 colleagues, 2008. Opaline silica in young deposits on Mars. Geology 36(11), 847–850. doi:10.1130/G24967A.1.
Milliken, R.E., Edgett, K.S., Swayze, G., Clark, R.N., Thompson, B.J., Anderson, R., Bell, J.F., 2009. Clay and sulfate-bearing rocks in a stratigraphic sequence in Gale Crater. Lunar Planet. Sci. Conf. XL. ID.1479.
Murchie, S.M., and 49 colleagues, 2007. Compact Reconnaissance Imaging Spectrometer for Mars (CRISM) on Mars Reconnaissance Orbiter (MRO). J. Geophys. Res. 112, E05S03. doi:10.1029/2006JE002682.
Murchie, S.M., and 15 colleagues, 2009a. A synthesis of martian aqueous mineralogy after 1 Mars year of observations from the Mars Reconnaissance Orbiter. J. Geophys. Res. doi:10.1029/2009JE003342.
Murchie, S.M., and 12 colleagues, 2009b. Evidence for the origin of layered deposits in Candor Chasma, Mars from mineral composition and hydrologic modeling. J. Geophys. Res. doi:10.1029/2009JE003343.
Murchie, S.M., and 19 colleagues, 2009c. The CRISM investigation and data set from the Mars Reconnaissance Orbiter's primary science phase. J. Geophys. Res. doi:10.1029/2009JE003344.
Mustard, J.F., Murchie, S.L., Erard, S., Sunshine, J., 1997. In situ compositions of martian volcanics: Implications for the mantle. J. Geophys. Res. 102, 25605–25615.
Mustard, J.F., and 35 colleagues, 2008. Hydrated silicate minerals on Mars observed by the CRISM instrument on MRO. Nature 454, 305–309.
Parente, M., 2008. A new approach to denoising CRISM images. Lunar Planet. Sci. Conf. XXXIX (Abstract #2528).
Pelkey, S.M., and 11 colleagues, 2007. CRISM multispectral summary products: Parameterizing mineral diversity on Mars from reflectance. J. Geophys. Res. 112, E08S14. doi:10.1029/2006JE002831.
Pelkey, S.M., Jakosky, B.M., Christensen, P.R., 2003. Surficial properties in Melas Chasma, Mars, from Mars Odyssey THEMIS data. Icarus 165 (1), 68–89.
Peulvast, J.-P., Masson, Ph.L., 1993a. Erosion and tectonics in central Valles Marineris (Mars): A new morphostructural model. Earth Moon Planet. 61, 191–217.
Peulvast, J.-P., Masson, Ph.L., 1993b. Melas Chasma: Morphology and tectonic patterns in central Valles Marineris (Mars). Earth Moon Planet. 61, 219–248.
Peulvast, J.-P., Mege, D., Chiciak, J., Costard, F., Masson, Ph.L., 2001. Morphology, evolution and tectonics of Valles Marineris wallslopes (Mars). Geomorphology 37, 329–352.
Pokrovski, G., Schott, J., Farges, F., Hazemann, J.-L., 2003. Iron (III)–silica interactions in aqueous solution: Insights from X-ray absorption fine structure spectroscopy. Geochim. Cosmochim. Acta 67 (19), 3559–3573.
Pollack, J.B., Kasting, J.F., Richardson, S.M., Poliakoff, K., 1987. The case for a wet, warm climate on early Mars. Icarus 71, 203–224. doi:10.1016/0019-1035(87)90147-3.
Poulet, F., Bibring, J.-P., Mustard, J.F., Gendrin, A., Mangold, N., Langevin, Y., Arvidson, R.E., Gondet, B., Gomez, C., and the OMEGA team, 2005. Phyllosilicates on Mars and implications for early martian climate. Nature 438. doi:10.1038/nature04274.
Poulet, F., Bibring, J.-P., Langevin, Y., Mustard, J.F., Mangold, N., Vincendon, M., Gondet, B., Pinet, P., Bardintzeff, J.-M., Platevoet, B., 2009a. Quantitative compositional analysis of martian mafic regions using MEx/OMEGA reflectance data: 1. Methodology, uncertainties and examples of application. Icarus 209, 69–83. doi:10.1016/j.icarus.2008.12.025.
Poulet, F.10 colleagues, 2009b. Quantitative compositional analysis of martian mafic regions using the MEx/OMEGA reflectance data: 2. Petrological implications. Icarus 201, 84–101. doi:10.1016/j.icarus.2008.12.042.
Quantin, C., Allemand, P., Mangold, N., Delacourt, C., 2004. Ages of Valles Marineris (Mars) landslides and implications for canyon history. Icarus 172, 555–572.
Roach, L.H., Mustard, J.F., Murchie, S.L., Bishop, J.L., Ehlmann, B.L., Lichtenberg, K., Parente, M., and the CRISM Science Team, 2009. Sulfate and hematite stratigraphy in Capri Chasma, Valles Marineris. Proc. Lunar Planet. Sci. Conf. XL. ID. 1826.
Schultz, R.A., 1998. Multiple-process origin of Valles Marineris basins and troughs, Mars. Planet. Space Sci. 46 (6/7), 827–834.
Sharp, R.P., 1973. Mars: Troughed terrain. J. Geophys. Res. 78, 4063–4072.
Smith, D.K., 1998. Opal, cristobalite, and tridymite: Noncrystallinity versus crystallinity, nomenclature of the silica minerals and bibliography. Powder Diffr. 13 (1), 2–19.
Smith, D.E., Zuber, M.T., Neumann, G.A., Guinness, E.A., Slavney, S., 2003. Mars Global Surveyor Laser Altimeter Mission Experiment Gridded Data Record, MGS-M-MOLA-5-MEGDR-L3-V1.0, NASA Planetary Data System.
Spenser, R.J., 2000. Sulfate minerals in evaporite deposits. In: Alpers, C.N., Jambor, J.L., Nordstrom, D.K. (Eds.), Sulfate Minerals: Crystallography, Geochemistry, and Environmental Significance. Reviews in Mineralogy, vol. 40. Mineral. Soc. Am, Washington, DC, pp. 173–192.
Stoffregen, R.E., Alpers, C.N., Jambor, J.L., 2000. Alunite-jarosite crystallography, thermodynamics, and geochemistry. In: Alpers, C.N., Jambor, J.L., Nordstrom, D.K. (Eds.), Sulfate Minerals: Crystallography, Geochemistry, and Environmental Significance, Reviews in Mineralogy, vol. 40. Mineral. Soc. Am., Washington, DC, pp. 453–479.
Swayze, G.A., Desborough, G., Smith, K., Lowers, H., Hammarstrom, J., Diehl, S., Leinz, R., Driscoll, R., 2008a. Understanding jarosite – From mine waste to Mars.

In: Verplanck, P.L. (Ed.), 2008b, Understanding Contaminants Associated with Mineral Deposits, vol. 1328. US Geol. Surv. Circular, pp. 8–13.
Swayze, G.A., and 12 colleagues, 2008b. Discovery of the Acid–Sulfate Mineral Alunite in Terra Sirenum, Mars, Using MRO CRISM: Possible Evidence for Acid–Saline Lacustrine Deposits? Eos Trans. AGU 89(53), Fall Meet. Suppl., Abstract P44A-04.
Tanaka, K.L., 1986. The stratigraphy of Mars. J. Geophys. Res. Suppl. 91, E139–58.
Tanaka, K.L., Golombek, M.P., 1989. Martian tension fractures and the formation of grabens and collapse feature at Valles Marineris. Proc. Lunar Planet. Sci. Conf. XIX, 383–396.
Tanaka, K.L., Golombek, M.P., Banerdt, W.B., 1991. Reconciliation of stress and structural histories of the Tharsis Region of Mars. J. Geophys. Res. 96 (E1), 15617–15633.
Tanaka, K.L., Scott, D.H., Greeley, R., 1992. Global stratigraphy. In: Kieffer, H.H., Jakosky, B.M., Snyder, C.M., Matthews, M.S. (Eds.), Mars. Univ. Arizona Press, Tucson, pp. 345–382.
Tosca, N.J., McLennan, S.M., 2006. Chemical divides and evaporite assemblages on Mars. Earth Planet. Sci. Lett. 241, 21–31.
Tosca, N.J., Milliken, R.E., Michel, F.M., 2008. Smectite formation on early Mars: Experimental constraints. Martian Phyllosilicates: Recorders of Aqueous Processes. Abstract 7030, 77–78.
Treiman, A.H., Fuks, K.H., Murchie, S.L., 1995. Diagenetic layers in the upper walls of Valles Marineris, Mars: Evidence for drastic climate change since the mid-Hesperian. J. Geophys. Res. 100 (E12), 26339–26399.
Treiman, A.H., 2008. Ancient groundwater flow in the Valles Marineris on Mars inferred from fault trace ridges. Nature Geosci. 1, 181–183. doi:10.1038/NGEO131.
Weitz, C.M., Parker, T.J., Blumer, M., Anderson, F.S., Grant, J.A., 2003. Geology of the Melas Chasma landing site for MER. J. Geophys. Res. 108(12), 8082. doi:10.1029/2002JE002022.
Weitz, C.M., Milliken, R., Grant, J., McEwen, A., Williams, R., Bishop, J.L., 2008. Light-toned strata and inverted channels adjacent to Juventae and Ganges Chasmata, Mars. Geophys. Res. Lett. 35, 19202. doi:10.1029/2008GL035317.
Williams, J.-P., Paige, D.A., Manning, C.E., 2003. Layering in the wall rock of Valles Marineris: Intrusive and extrusive magmatism. J. Geophys. Res. 30(12), 1623. doi:10.1029/2003GL017662.
Wiseman, S.M., Arvidson, R.E., Morris, R.V., Murchie, S.L., Seelos, F.P., Andrews-Hanna, J.C., and the CRISM Team, 2009. Hydrated sulfate deposits detected within Schiaparelli Crater, Mars. Lunar Planet. Sci. Conf. XL. ID. 1798.
Wray, J.J., Ehlmann, B.L., Squyres, S.W., Mustard, J.F., Kirk, R.L., 2008a. Compositional stratigraphy of clay-bearing layered deposits at Mawrth Vallis, Mars. Geophys. Res. Lett. 35, L12202. doi:10.1029/2008GL034385.
Wray, J.J., Milliken, R.E., Murchie, S.L., Swayze, G.A., Dundas, C.M., Seelos, F.P., Squyres, S.W., 2008b. Clays and Sulfates in a Potential Lacustrine Evaporite Sequence at Columbus Crater, Mars. Eos Trans. AGU 89(53), Fall Meet. Suppl., Abstract P53B-1446.
Zuber, M.T., Smith, D., Solomon, S., Muhleman, D., Head, J., Gravin, J., Abshire, J., Bufton, J., 1992. The Mars Observer Laser Altimeter investigation. J. Geophys. Res. 97 (5), 7781–7797.